



**fire**  
cci

---

## ESA Climate Change Initiative – Fire\_cci D5.1 Climate Assessment Report (CAR)

---

<b>Project Name</b>	ECV Fire Disturbance: Fire_cci
<b>Contract N°</b>	4000126706/19/I-NB
<b>Issue Date</b>	16/11/2020
<b>Version</b>	2.1
<b>Author</b>	Angelika Heil, Idir Bouarar
<b>Document Ref.</b>	Fire_cci_D5.1_CAR_2.1
<b>Document type</b>	Public

*To be cited as: Heil A., Bouarar I. (2020) ESA CCI ECV Fire Disturbance: D5.1  
Product Validation and Intercomparison Report, version 2.1. Available at:  
<https://climate.esa.int/en/projects/fire/key-documents/>*

 <b>fire</b> cci	<b>Fire_cci</b>		Ref.	Fire_cci_D5.1_CAR_v2.1		
	<b>Climate Assessment Report</b>		Issue	2.1	Date	16/11/2020
				Page	2	

## Project Partners

Prime Contractor/ Scientific Lead & Project Management	UAH – University of Alcalá (Spain)
Earth Observation Team	UAH – University of Alcalá (Spain) UPM – Universidad Politécnica de Madrid (Spain) CNR-IREA - National Research Council of Italy – Institute for Electromagnetic Sensing of the Environment (Italy)
System Engineering	BC – Brockmann Consult (Germany)
Climate Modelling Group	MPIM – Max Planck Institute for Meteorology (Germany) CNRS - National Centre for Scientific (France)



## Distribution

Affiliation	Name	Address	Copies
ESA	Clément Albergel (ESA)	clement.albergel@esa.int	electronic copy
Project Team	Emilio Chuvieco (UAH) M. Lucrecia Pettinari (UAH) Joshua Lizundia (UAH) Gonzalo Otón (UAH) Mihai Tanase (UAH) Consuelo Gonzalo (UPM) Dionisio Rodríguez Esparragón (UPM) Daniela Stroppiana (IREA) Mirco Boschetti (IREA) Thomas Storm (BC) Angelika Heil (MPIM) Idir Bouarar (MPIM) Florent Mouillot (LSCE) Philippe Ciais (LSCE)	emilio.chuvieco@uah.es mlucrecia.pettinari@uah.es joshua.lizundia@uah.es gonzalo.oton@uah.es mihai.tanase@uah.es consuelo.gonzalo@upm.es dionisio.rodriquez@ulpgc.es stroppiana.d@irea.cnr.it boschetti.m@irea.cnr.it thomas.storm@brockmann-consult.de angelika.heil@mpimet.mpg.de idir.bouarar@mpimet.mpg.de florent.mouillot@cefe.cnrs.fr philippe.ciais@lsce.ipsl.fr	electronic copy

 <b>fire</b> cci	<b>Fire_cci</b> <b>Climate Assessment Report</b>		Ref.	Fire_cci_D5.1_CAR_v2.1		
			Issue	2.1	Date	16/11/2020
			Page		3	

## Summary

This document is the version 2.0 of the Climate Assessment Report for the Fire\_cci project. It refers to Task 5, Work Package 5100 – Atmospheric Emissions. This document is a completely new version compared to the previous one, focusing on the user case of the applications of the ECV products, in this case assessing the FireCCISFD11 burned area product related to atmospheric emissions.

	Affiliation/Function	Name	Date
<b>Prepared</b>	MPIM	Angelika Heil Idir Bouarar	16/11/2020
<b>Reviewed</b>	UAH – Project Manager UAH - Science Leader	M. Lucrecia Pettinari Emilio Chuvieco	16/11/2020
<b>Authorized</b>	UAH - Science Leader	Emilio Chuvieco	16/11/2020
<b>Accepted</b>	ESA - Technical Officer	Clément Albergel	16/11/2020

This document is not signed. It is provided as an electronic copy.

## Document Status Sheet

Issue	Date	Details
<b>1.0</b>	31/03/2017	First Document Issue
<b>1.1</b>	30/09/2017	Revised document, including answers to the comments on CCI-FIRE-EOPS-MM-17-0045, new analysis, and the inclusion and analysis of Sentinel-2 SFD BA information.
<b>1.2</b>	23/04/2018	Revised document, including answers to the comments on CCI-FIRE-EOPS-MM-18-0004, and new analysis of the MODIS Fire_cci v5.0 product.
<b>1.3</b>	22/06/2018	Revised document, including answers to the comments on CCI-FIRE-EOPS-MM-18-0159
<b>1.4</b>	16/11/2018	Update of the document
<b>2.0</b>	06/11/2020	Update of the whole content of the document
<b>2.1</b>	16/11/2020	Revised document, including answers to the comments on Fire_cci+_5.1_CAR_v2.0_RID

## Document Change Record

Issue	Date	Request	Location	Details
1.1	30/09/2017	ESA, LSCE-IRD	Summary Figures 3 and 4 Section 3.1 Section 3.2, Section 4. Conclusion	Update of the summary of the document. Figures updated to include MCD64A1. Minor changes in the text The sections have been expanded with new analyses and new datasets. The conclusions were updated to include the new analyses performed.
1.2	23/04/2018	ESA, LSCE-IRD	Summary Section 1 Section 2 Section 3 Section 3.1 Section 3.2  Section 4.1 Section 4.2.1	Update of the summary of the document. Small changes in the text to address MODIS Fire_cci v5.0. Parameter units corrected, and ellipse main features expanded. Text expanded Small changes in the text. The analysis was changed to include MCD64A1 C6 instead of MCD45A1 C5. The figures and text were updated. Small changes in the text. Text updated (was previously Section 4.2)

			Section 4.2.2 Section 4.4 Section 6	New section added Added comparison of SFD and MCD64A1 Conclusions updated
1.3	22/06/2018	ESA, LSCE-IRD	All document Figure 1 Figure 5 Section 3.2	Inclusion of acronyms of the products. Figure updated Caption updated Clarification added to the first paragraph.
1.4	16/11/2018	LSCE-IRD	All document Sections 3.3, 5.3 Sections 4.2.1, 4.4 Section 4.2.2 Previous Sections 5.1 and 5.2 Section 6	Inclusion of FireCCI51 analysis New sections added Small changes in the text Text updated to include FireCCI51 Sections replaced by new Section 5.1 Text updated
2.0	06/11/2020	MPIM	All document	All document updated
2.1	16/11/2020	ESA	Sections 2.1, 4.5.1  Section 3 Section 4.3 Sections 4.4.2, 5	Small changes in the text and Figure legends updated Table 2 expanded Text expanded Small changes in the text

## **Table of Contents**

<b>1. Executive Summary</b> .....	<b>8</b>
<b>2. Introduction</b> .....	<b>8</b>
2.1. Vegetation fires in Africa .....	9
2.2. Burned area estimates for Africa.....	10
<b>3. WRF-Chem model and setup</b> .....	<b>11</b>
3.1. Anthropogenic emissions .....	12
<b>4. Fire emission inventories used in this study</b> .....	<b>14</b>
4.1. FINN .....	15
4.2. GFED4s.....	15
4.3. FireCCISFD11-derived fire emissions.....	16
4.3.1. Fuel consumption.....	17
4.3.2. Fuel type stratification .....	19
4.3.3. Emission factors.....	20
4.4. Pre-processing fire emission inputs for WRF-Chem .....	23
4.4.1. Diurnal cycle.....	23
4.4.2. Day-to-day variability .....	24
4.4.3. Remapping to the curvilinear model grid .....	25
4.4.4. Fire size distribution for WRF-Chem plume rise calculation.....	26
4.5. Fire Emission Estimates for Africa .....	29
4.5.1. Sensitivity of emission estimation to fuel type parameterisation .....	32
<b>5. WRF-Chem model evaluation</b> .....	<b>34</b>
<b>6. Conclusions</b> .....	<b>37</b>
<b>7. References</b> .....	<b>39</b>
<b>Annex 1: Acronyms and abbreviations</b> .....	<b>48</b>

## **List of Tables**

Table 1: Monthly area burned in Africa (in Mha) estimated by different satellite-derived burned area products throughout July to September 2016. ....	11
Table 2: WRF-Chem model configuration used in this study. ....	12
Table 3: Emission factors used to calculate FireCCISFD11 fire emissions (in g per kg dry matter burned). 'tracer' identifies to which WRF-Chem tracers the species is mapped. ....	21
Table 4. Emission factors for carbon monoxide (CO), oxides of nitrogen (NO <sub>x</sub> ) and black carbon (BC) (in g per kg biomass burned) used in different fire emission inventories. N.B. FireCCISFD11 uses the GFED4s emission factors. ....	22
Table 5: Monthly total number of individual fires identified in Africa in different burned area products (in thousand). ....	27
Table 6: Total emissions of carbon monoxide (CO), oxides of nitrogen (NO <sub>x</sub> ) and black carbon (BC) emitted from vegetation fires in Africa throughout July to September 2016 (in Tg), as estimated by various satellite-derived inventories. Estimates of anthropogenic emissions are shown for comparison. ....	29
Table 7: Pearson's correlation values (r <sup>2</sup> ) between time series of daily total CO emission from fires in Africa (July to September 2016). ....	32
Table 8: Fuel consumption (FC) and emission factors (EF) estimates from the Andreae (2019) and van Leeuwen et al. (2014) compilations for the four major fuel types in Africa. The first three columns depict how the CCI S2 and the LC_cci v2.0.7 land cover classes are translated. ....	34
Table 9: Total emissions from fires across Africa during the period July to September 2016 calculated from FireCCISFD11 burned area using different fuel type parameterisations (see Table 8). ....	34

## **List of figures**

Figure 1: (a) FirecciSFD11 burned area per 0.25° grid cell in the calendar year 2016 displayed in the geographical bounds of the WRF-Chem model domain used in this study and (b) FireCCISFD11 monthly burned area in Africa north of the Equator (NHAF) and south of the Equator (SHAF), respectively. WRF-Chem simulations in this study cover the period from mid-June to end of September 2016. Data extracted from the Fire_cci Small Fire Database (SFD) Burned Area grid product, version 1.1. ....	9
Figure 2: (a) EDGAR432 PM <sub>2.5</sub> to OC ratio map calculated for the road transport sector (TRO) for the year 2010. (b) Scatterplot showing the relation between monthly EDGAR432 road transport emissions of OC and PM <sub>2.5</sub> for Africa for the year 2010. ....	13
Figure 3: Burned area in September 2016 (in ha per 0.1° grid) (a) agricultural waste burning in CAMS41 based on agricultural statistics and (b) and (c) vegetation fires detected from satellites (FireCCISFD11: Sentinel -2A burn scar detection; FINN: MODIS active fire). ....	14

- Figure 4: Flowchart illustrating how fire emissions are constructed from the gridded FireCCISFD11 burned area product and how they are pre-processed to comply with the specifications of WRF-Chem fire emission input data..... 17
- Figure 5: (a) GFED4s-based fuel consumption layer for the study domain for July 2016 (kg fuel per m<sup>2</sup> burned). Only shown are grid cells with non-zero fire activity in the FireCCISFD11 July data. (b) JAS 2016 mean GFED4s fuel consumption across southern hemispheric Africa (in kg fuel per m<sup>2</sup> burned). Only shown are grid cells where GFED4s exhibits fire activity in all three months. (c) Absolute deviation of GFED4s monthly fuel consumption from the July to September mean (in %). The colour levels correspond to the 10, 25, 50, 75 and 90 field percentiles. .... 19
- Figure 6: (a-c) GFED4s-based fuel type partitioning layer for the southern hemispheric regions of the study domain (JAS 2016 mean) expressing the fractional contribution of fuel types to total fuel consumption. Shown are grid cells where the FireCCISFD11 product records fire activity in JAS 2016. SAVA, AGRI and DEFO stands for savanna, agriculture, deforestation fires, respectively. .... 20
- Figure 7: Parameterization of the diurnal emission profile in FINN and GFED4s. The GFED4s profile is extracted from the 3-hourly GFED4s diurnal\_cycle data layer for July 2016. Only data points with active fires in the WRF-Africa model domain are included. The boxplots reflect the diurnal cycle variability within this domain, the mean GFED4s diurnal cycle profile is indicated by a black dot. The FINN diurnal profile is extracted from the fire\_emis preprocessor. .... 24
- Figure 8: (a-c) Observational coverage in the FireCCISFD11 product during July to September 2016, expressed as fraction of the burnable area within each 0.25° grid cell for which valid satellite observations were available. The FireCCISFD11 product covers continental Africa south of 25° N. Low observational coverage between 15° and 25° N is related to the presence of unburnable land cover. (d) Day of burn computed from the FireCCISFD11 pixel product for the period 1<sup>st</sup> – 10<sup>th</sup> September 2016. The coloured bands reflect the 290 km swath width of the MSI-LIC sensor. Rectangles in (c) and (d) highlight observational gaps occurring in the proximity of fires. .... 25
- Figure 9: FirecciSFD11 burned area in September 2016 (a) original 0.25° grid product and (b)-(c) original grid product interpolated to the WRF-Chem grid with bilinear and conservative remapping, respectively, and (d) pixel product interpolated to WRF-Chem grid (with conservative remapping). Number show total burned area across Sub-Saharan Africa..... 26
- Figure 10: (a) Absolute and (b) relative difference between FireCCISFD11 burned area mapped to the WRF-Chem curvilinear grid from the pixel product ("pix", see also Figure 9c) and from the grid product ("cons", see also see also Figure 9d). (c) Gridded fire size distribution (i.e. burned area per grid and month) in the different remapping schemes (see also Figure 9)..... 26
- Figure 11: (a) Cumulative histogram of FINN mean hourly fire size per WRF grid for the individual fuel type classes (period July to September 2016). (b) Boxplots of mean fire size per WRF grid by fuel type. Red marker denotes the arithmetic mean size. (c) Contribution of FINN fuel types to total burned area calculated from the WRF mean fire size variable for the WRF-Chem Africa domain. The following abbreviations are used: EF=extratropical forest, TF=tropical forest, GR=grassland, SV=savanna. ALL is the total fire size per WRF (sum over the four fuel type classes). .... 28

Figure 12: Same as Figure 11, but for GFED4s. ....	28
Figure 13: Same as Figure 11, but for FireCCISFD11.....	28
Figure 14: Monthly total emissions from fires across Africa (in Tg) during July to September 2016 estimated by different inventories (a) carbon monoxide (CO) and (b) oxides of nitrogen (NO <sub>x</sub> ) as NO, and (c) black carbon (BC). Anthropogenic emissions from the CAMS-ANTHRO inventory are shown as well. ....	30
Figure 15: Daily total emissions from fires across Africa (in Gg) during July to September 2016 (a) carbon monoxide (CO), (b) black carbon (BC) and (c) oxides of nitrogen (NO <sub>x</sub> as NO). ....	31
Figure 16: Hourly total emissions from fires across Africa (in Gg) in the first half of August 2016 (a) carbon monoxide (CO), (b) black carbon (BC) and (c) oxides of nitrogen (NO <sub>x</sub> as NO). ....	31
Figure 17: Dominant land and fuel cover type in grid cells with FireCCISFD11 fire detections across JAS 2016 using (a) ESA CCI S2 land cover map, (b) the GFED4s fuel partitioning layer, and (c) a translated ESA CCI LC_cci v2.0.7 land cover map of the year 2015. The translation largely follows ESA (2017), Wang et al. (2019) and Tab. 7 of Bai (2010). Grassland savanna (GSAV) corresponds to the UN-LCCS land cover classes 130 to 150, woody savanna (WSAV) to the classes 60, 110, 120 and 180, and agriculture (AGRI) the classes 10 to 40. The LC_cci v2.0.7 product consists of annual maps. To classify the land cover type burned across JAS2016, the land cover map of the year 2015 is used since it better reflects the land cover prior the JAS2016 fires than the land cover map of the year 2016. ....	33
Figure 18: (a) Surface carbon monoxide (CO) concentrations modelled with WRF-Chem for June 18, 2016 with FINN fire emissions (reference run). Relative difference with respect to the reference run when using (b) GFED4s and (c) FireCCISFD11 fire emissions. ....	34
Figure 19: (a) Topographic map of the WRF-Chem Africa model domain with line along 19° E indicating the cross-section displayed in (b) and (c). Cross-section showing the vertical distribution of modelled carbon monoxide concentrations for June 18, 2016. Shown is the absolute difference of the simulation with (b) GFED4s and (c) FireCCISFD11 fire emissions, respectively, and the FINN reference run. ....	35
Figure 20: Comparison of CO concentrations modelled by WRF-Chem in the reference run (FINN fire emissions) with those measured by the DACCIIWA aircraft measurement campaign on July 2, 2016 over coastal Ghana. (a) displays the flight track including flight height and latitude information, and (b) the concentrations along the flight track. ....	36
Figure 21: Comparison of CO atmospheric columns modelled by WRF-Chem in the reference run (FINN fire emissions) with MOPITT observations for July 2016. ...	36

 <b>fire</b> cci	<b>Fire_cci</b>		Ref.	Fire_cci_D5.1_CAR_v2.1		
	<b>Climate Assessment Report</b>		Issue	2.1	Date	16/11/2020
					Page	8

## 1. Executive Summary

Fire emission inventories for Africa still differ largely. This uncertainty is a major constraint for accurately characterizing the impact of fires in Africa on air quality and climate. Fire emission inventories rely on different satellite products of burned area (BA), hotspot (HS) or fire radiative power (FRP). Also, the assumed type of vegetation burned, fuel consumption and emission factors vary amongst inventories. The recently released 20-m Sentinel-2 BA product FireCCISFD11 can resolve small fires that are largely omitted in the most widely used MODIS-based fire emission products.

We performed simulations over Africa with the regional atmospheric chemistry transport model WRF-Chem using three fire emission inventories as boundary condition. Firstly, the WRF-Chem default fire emission inventory FINN, which relies on MODIS hotspots. Secondly, GFED4s, which is the emission inventory most widely used in atmospheric chemistry applications and which bases upon MODIS burned area. Thirdly, a newly created fire emission inventory using FireCCISFD11 burned area information. For the two latter, a WRF-Chem pre-processor was created to convert the emission inventories into WRF-Chem input fields.

The preliminary evaluation of WRF-Chem model results against satellite and aircraft observations indicates an over-prediction of atmospheric concentrations when using GFED4s and FireCCISFD11 fire emissions. Further analysis will focus on elucidating the causes for the observed bias.

## 2. Introduction

This document explores the usage of Fire\_cci burned area products for providing fire emission input information to regional atmospheric chemistry models. So far, Fire\_cci burned area products have not yet been applied in this area of research. Atmospheric chemistry models are widely used to study the dispersion of emissions, to predict air quality, to apportion emission sources to local air pollution, and, when combined with independent measurements of atmospheric constituents, to constrain bottom-up emission inventories, including those from biomass burning (e.g. Nurzahziani et al., 2020).

To predict fire-related atmospheric concentrations of chemical trace species and aerosols, we performed simulations with the regional Weather Research Forecasting model coupled with Chemistry (WRF-Chem) using different fire emission inventories as boundary condition. WRF-Chem simulates the atmospheric transport, mixing, and chemical transformation of the emissions simultaneously with the meteorology. The comparison of modelled atmospheric concentrations with measurements of atmospheric trace species is a means to constrain bottom-up fire emission inventories.

This study focuses on the atmospheric implications of emissions from fires in Africa. Vegetation fires lead to widespread severe air pollution in Africa entailing an estimated 43 000 premature deaths every year (Bauer et al., 2019). Transatlantic transport of African biomass burning emissions, which particularly occurs during the southern hemispheric peak fire season, not only affects air quality in South America, but also affects cloud formation across the Amazon (Holanda et al., 2020). Yet, the large uncertainties in the fire emission estimates for Africa render it difficult to quantitatively assess the full range of atmospheric impact (Williams et al., 2012; Zhang et al., 2014).

Estimating fire emissions requires information on the area burned, the amount of fuel consumed per unit area burned, and the trace species emission factors. Knowledge on these parameters from field observations is scarce, especially for fires in remote areas

such as the African savanna, which is why various estimation approaches come into play. One approach is to generalise the few measurements available and derive best-guess parameter estimates. For fuel consumption, the other approach is to use a data-driven biogeochemical model, as done in the Global Fire Emission Database (GFED) framework. The advantage of the model is that it can capture the seasonal and inter-annual changes in fuel consumption along with e.g. rainfall variability (Scholes et al., 2011), while the best-guess parameters are static.

In this study, we use WRF-Chem to evaluate fire emission estimated from the FireCCISF11 burned area product by adopting the fuel consumption and emission factor parameterisation from the latest GFED version 4s. We compare the results with model simulations that use FINN, the default fire emission inventory in WRF-Chem, and GFED4s fire emission.

## 2.1. Vegetation fires in Africa

Fire is an integral part of the African ecosystem affecting roughly 10% of Africa's land surface every year (Figure 1a)(van der Werf et al., 2017). The African fire regime is characterised by two distinct fire seasons: one during July to September where most fires burn in the southerly tropical regions and another between November and January where fires in the northern tropics predominate (Figure 1b). Most fires in Africa are savanna fires. Agricultural fires related to in-field residue burning or deforestation fires play a minor role. Savannas, characterised by sparsely tree covered grass- or woodlands, dominate vast regions of tropical and subtropical Africa. Savannas are fire-adapted; the fires typically only consume fuels in the ground layer surface fuels, leaving the trees unaffected. The surface fuels, in turn, rapidly regrow, ensuring sufficient fuel for the next burning (Osborne et al., 2018; Ratnam et al., 2011). Fire spread in African savannas is fuel-limited, and not dryness-limited (Kahiu and Hanan, 2018; Scholes et al., 2011). In addition, people in Africa use the landscape intensively for agriculture and grazing, thereby decreasing and fragmenting fuel loads, and, in consequence, lowering fire spread and fuel consumption.

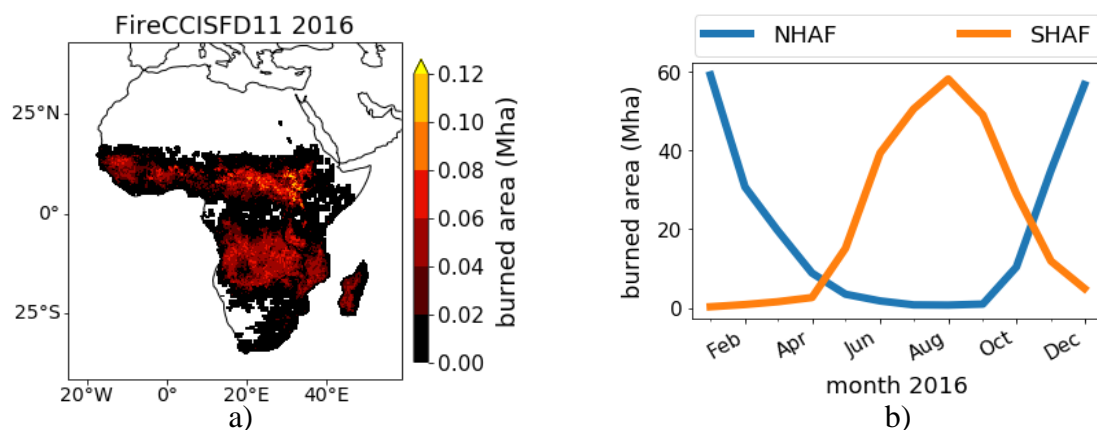


**Figure 1:** (a) FireCCI\_SFD11 burned area per 0.25° grid cell in the calendar year 2016 displayed in the geographical bounds of the WRF-Chem model domain used in this study and (b) FireCCI\_SFD11 monthly burned area in Africa north of the Equator (NHAF) and south of the Equator (SHAF), respectively. WRF-Chem simulations in this study cover the period from mid-June to end of September 2016. Data extracted from the Fire\_cci Small Fire Database (SFD) Burned Area grid product, version 1.1.

Fire activity across Africa has substantially declined over the past two decades, triggered by climatic and socio-economic changes (Andela et al., 2017; Zubkova et al., 2019). Yet,

 <b>fire</b> cci	<b>Fire_cci</b>		Ref.	Fire_cci_D5.1_CAR_v2.1		
	<b>Climate Assessment Report</b>		Issue	2.1	Date	16/11/2020
					Page	10

Africa is still by far the largest continental contributor to global burned area and fire emissions (van der Werf et al., 2017).

Fire emission inventories for Africa are, however, subject to considerable uncertainty. As field observations of fires are lacking, the inventories rely on satellite observations of burned area, active fire pixels ('hotspots') or fire radiative power (FRP). Most satellite observations, due to the coarse spatial resolution of the underlying sensors, cannot resolve small fires (< 100 ha), and also cannot detect fires through thick cloud or smoke cover, resulting in an underrepresentation of these fires in emission inventories (Randerson et al., 2012; van der Werf et al., 2017).

Most fire emission inventories for Africa rely on burned area estimates, which build either upon direct burn scar observations, such as e.g. AMMABB (African Monsoon Multidisciplinary Analysis Biomass Burning, Lioussé et al., 2010), GFED (Global Fire Emissions Database, van der Werf et al., 2010, 2017) or on hotspot observations that are translated into burned area, such as e.g. the Fire INventory from NCAR (FINN, Wiedinmyer et al., 2011). Burned area is then combined with fuel consumption estimates to derive biomass combustion rates and subsequently fire emission fluxes. Estimating biomass combustion rates directly from FRP observations is an alternate approach used e.g. in the Global Fire Assimilation System (GFAS, Kaiser et al., 2012). In contrast to these 'bottom-up' emission inventory approaches, 'top-down' methods used e.g. in FEER (Fire Energetics and Emissions Research, Ichoku and Ellison, 2014), QFED (Quick Fire Emissions Dataset, Darmenov and da Silva, 2015) or FREM (Fire Radiative Energy Emissions, Nguyen and Wooster, 2020) bypass the largely uncertain fuel consumption estimation step by directly estimating emission fluxes from FRP observations. Top-down methods derive 'smoke emission coefficients' by quantitatively linking the FRP of an individual fire or fire cluster with satellite retrievals of aerosol optical depth (AOD) of the corresponding smoke plume. This linkage, however, has its own uncertainties, caused by e.g. unknowns in how to translate AOD to particulate matter emission fluxes (Li et al., 2019, 2020; Lu et al., 2019; Nguyen and Wooster, 2020).

In their intercomparison, Pan et al. (2020) show that, at a global scale, the two 'top-down' inventories QFED and FEER have a factor of 2-4 larger aerosol emissions than the bottom-up inventories FINN, GFAS, GFED3 and GFED4s. The discrepancies with bottom-up inventories are most pronounced in QFED; in regions such as boreal or temperate North America or Australia, QFED aerosol emissions are at least 10 times higher than in the bottom-up inventory with the lowest estimate.

## 2.2. Burned area estimates for Africa

Different satellite-based burned area estimates for Africa are commonly up to a factor of two apart (Table 1). Burned area estimates tend to be higher in burn scar observations from optical sensors with higher spatial resolution because smaller fires tend to be better captured. The MODIS MCD64A1 burned area products (Giglio et al., 2013, 2018; van der Werf et al., 2017), for example, rely on observations at 500 m resolution, the FireCCI51 burned area estimates (Lizundia-Loiola et al., 2020) are based on 250-m MODIS observations, and in the FireCCISFD11 product (Roteta et al., 2019), burned area is mapped from 20-m spatial resolution MSI-L1C images acquired by the Sentinel-2A satellite. All these burned area products rely on a hybrid mapping algorithm, in which surface reflectance imagery are supplemented with satellite detections of active fires to enhance the probability of capturing fire events. In contrast, the operational burned area product of the Copernicus Global Land Service (CGLS, Tansey, 2020) solely relies on

333 m resolution PROBA-V surface reflectance imagery and burned area in FINN (Wiedinmyer et al., 2011) is indirectly only derived from 1 km resolution MODIS active fire information.

We compare burned area estimate for Africa for the July to September fire season of the year, i.e. the only year for which FireCCISFD11 burned area estimates are available. Compared to the precedent 15 years, the year 2016 was below average in terms of annual burned area in Africa and also in terms of July to September totals (Table 1).

Table 1 shows that FireCCISFD11 monthly burned area estimates for Africa in the study period July to September 2016 are by a factor of 1.8 to 2.3 larger than GFED4, which is equivalent to the MCD64A1 Collection 5 standard burned area product, and by a factor of around 1.75 larger than the estimates in the improved version of this product (i.e. MCD64A1 Collection 6). Even when compared to GFED4s, in which the GFED4 burned area is increased by a burned area estimate from unresolved small fires, FireCCISFD11 burned area is still around 55% higher. Total GFED4s burned area, in turn, is largely similar to the FireCCI51 and FINN estimates.

**Table 1:** Monthly area burned in Africa (in Mha) estimated by different satellite-derived burned area products throughout July to September 2016.

Mha	FireCCISFD11	FINNv1.5	GFED4s	GFED4 <sup>a</sup>	FireCCI51	MCD64C6 <sup>b</sup>	CGLSv1
Jul-16	51.2	35.0	33.8	25.2	39.7	28.7	20.8
Aug-16	58.7	38.5	36.8	25.9	32.9	33.6	21.0
Sep-16	49.8	26.1	32.2	27.0	31.7	28.4	13.5
total	159.7	99.5	102.9	78.1	104.2	90.6	55.2
year 2016	490.1	269.1	300.9	228.5	311.2	272.8	177.7
mean 2001/15	–	281.5 <sup>c</sup>	328.0	237.1	320.8	284.7	–

<sup>a</sup> GFED4 is the unboosted GFED4s product and corresponds to a 0.25° gridded version of the MCD64A1 Collection 5 burned area product. <sup>b</sup> MCD64A1 Collection 6. <sup>c</sup> 2002-2015 mean annual total.

We here explore to what extent the larger burned area in FireCCISFD11 translates into enhanced fire emission fluxes and investigate, by means of WRF-Chem model simulations, what the atmospheric implications of the enhanced fire emissions are compared to the most widely used fire emission inventories GFED4s and FINN.

### 3. WRF-Chem model and setup

WRF-Chem is a Weather Research and Forecasting (WRF) model coupled with Chemistry (Grell et al., 2005). It is widely applied for regional air quality and atmospheric chemistry studies (Bouarar et al., 2019; Kuik et al., 2015), including those specifically focussing on biomass burning emissions (Crippa et al., 2018; Grell et al., 2011; Nurzahziani et al., 2020). WRF-Chem simultaneously simulates the turbulent mixing, transport, transformation, and deposition of trace gases and aerosols emitted into the atmosphere.

WRF-Chem has an optional plume rise module implemented to distribute fire emissions vertically in the atmosphere. The module requires information on the instantaneous fire size and the fuel type distribution at the grid level. The fire size is used to estimate the plume radius. The fuel type determines the fire's heat flux and the resultant convective

energy. Default lower and upper bound heat flux values (in kW per m<sup>2</sup> area burned) for four fuel categories are prescribed: grasslands, savanna, tropical forest and boreal forest. From this information, the plume rise module calculates the lower and upper injection height of fire emissions.

The WRF-Chem version v4.1.2 was set up over the entire continental Africa with a horizontal resolution of around 18 km and 36 vertical levels. The model domain spans from 21°W to 55°E longitude and 37.5°S to 39°N latitude. The simulations cover the period mid-June to September 2016 where wide areas of southern tropical Africa are subject to fire. Table 2 specifies the model configuration used.

**Table 2:** WRF-Chem model configuration used in this study.

<b>WRF-Chem model configuration</b>	
model version	4.2.1
gas-phase chemistry	MOZART-4
aerosol chemistry	GOCART bulk aerosol
boundary conditions	meteorology: NCEP reanalysis chemistry: ECMWF-CAMS
biogenic emissions	MEGAN online
anthropogenic emissions	CAMS-ANTHROv4.1
biomass burning emissions	FINNv1.5 (reference simulation) GFED4s FireCCISFD11
model domain	21°W–55°E, 37.5°S–39°N

### 3.1. Anthropogenic emissions

To provide anthropogenic emission input to the WRF-Chem model, we use the CAMS-ANTHRO v4.1 inventory, here abbreviated with CAMS41. CAMS41 provides global, 0.1° degree gridded monthly emission estimates for twelve separate anthropogenic sectors for the period 2000 to 2019 (Elguindi et al., 2020; Granier et al., 2019). As WRF-Chem input, we selected emissions for the period June to September 2016 for the Africa model domain (Table 2).

CAMS41 contains emission estimates for the aerosol components black carbon (BC) and organic carbon (OC), but no estimates of PM<sub>10</sub> or PM<sub>2.5</sub>, which refers to particulate matter (PM) smaller than 10 or 2.5 μm aerodynamic diameter, respectively. Since all four aerosol components are a required input to WRF-Chem, we use the following scaling approach to estimate anthropogenic CAMS41 PM<sub>2.5</sub> and PM<sub>10</sub> emissions: CAMS41 represents a temporal extension of the EDGAR v4.3.2 inventory (in short: EDGAR432) (Crippa et al., 2018). Annual CAMS41 emissions in 2010 are basically identical with the year 2010 EDGAR432 emissions, when translating the EDGAR432 sectors to the CAMS41 sectors as indicated in (Granier et al., 2019). In contrast to CAMS41, EDGAR432 provides emissions for all four aerosol components. We found that in EDGAR432, PM<sub>2.5</sub> emission fluxes in the individual sectors are strongly linearly linked to the BC and/or OC emission flux patterns (see e.g. Figure 2). Also PM<sub>10</sub> emission fluxes were largely linearly related to the PM<sub>2.5</sub> emission fluxes. The relationship is constant over the individual months of the year. Dependent upon the sector, we created either maps with the PM<sub>2.5</sub> to OC or PM<sub>2.5</sub> to BC ratio, and applied these maps upon the CAMS41 OC or BC emission fields of the same sector. Subsequently, we applied the EDGAR432 PM<sub>10</sub> to PM<sub>2.5</sub> ratio map to create CAMS41 PM<sub>10</sub> emission. For the AGL (agriculture livestock) sector, we used the PM<sub>2.5</sub> to NH<sub>3</sub> ratio for scaling. For the AGS

(agricultural soil) sector, scaling based on a ratio map was not possible and we therefore extrapolated the EDGAR432 PM<sub>2.5</sub> and PM<sub>10</sub> emissions of the year 2012 to the year 2016 based on the temporal trend that was deduced from the 2010 to 2012 time series.

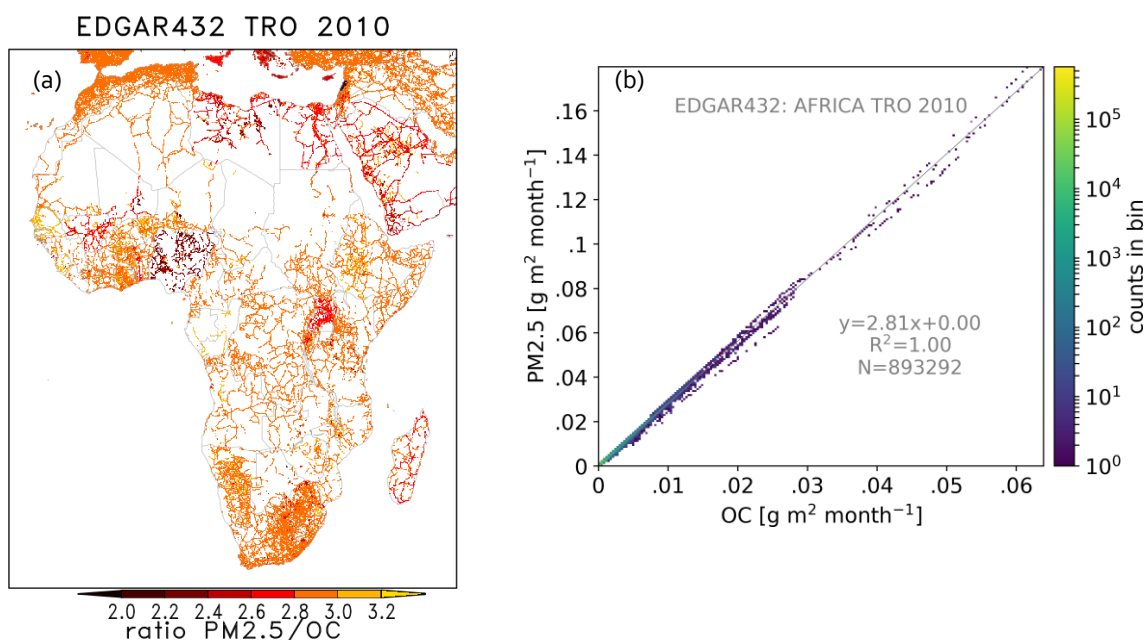


**Figure 2:** (a) EDGAR432 PM<sub>2.5</sub> to OC ratio map calculated for the road transport sector (TRO) for the year 2010. (b) Scatterplot showing the relation between monthly EDGAR432 road transport emissions of OC and PM<sub>2.5</sub> for Africa for the year 2010.

The anthropogenic CAMS41 agricultural waste burning (AWB) sector includes emissions from field burning of agricultural residues. These emissions are estimated from agricultural statistics and, by intent, exclude savanna fires (Janssens-Maenhout et al., 2019). Crippa et al. (2018) raises the problem of double-counting emission from agricultural fires when merging them with satellite-derived biomass burning emission inventories. The latter primarily cover large-scale vegetation fires, but to some extent, also smaller agricultural fires. We estimate the approximate area burned by cropland fires in CAMS41 from the CAMS41 AWB carbon monoxide (CO) emissions using the average FINN CO emission rate for cropland fires for Africa of 82.2 g CO per m<sup>2</sup> burned. From this, we estimate a total burned area of 1.95 Mha across Africa during July to September (JAS) 2016, which is roughly 1-2% of the satellite-derived burned area estimates. Most of the CAMS41 agricultural fires take place in regions where satellite-derived burned area products detect no fires (Figure 3). For example, there are abundant agricultural fires in West Africa in CAMS41 which are not detected in FireCCISFD11, despite the latter resolving fires as small as 0.04 ha, pointing to inaccuracies in the agricultural calendar used to construct CAMS41 fire emissions. To roughly assess the relevance of a double-counting of agricultural fires, we intersect CAMS41 AWB with FireCCISFD11 and FINN data for JAS 2016 at the monthly, 0.1° gridded level. We note that in around 75% of the grid cells with fire activity in FireCCISFD11 or FINN, there are concurrent agricultural fires in CAMS41. However, in these grid cells, their contribution to the total satellite-derived burned area is only around 0.4%, and, in terms of total fire-related CO emissions, less than 0.001%. Reversely, only 35% and 21% of the grid cells with agricultural fires in CAMS41 have concurrent fire observations in FireCCISFD11 and FINN, and most CO cropland fire emissions (69% and 85%, respectively) have no overlap with satellite-derived fire emissions. Overall, the double-counting of agricultural emissions when

combining CAMS41 anthropogenic emission inventory with satellite-derived biomass burning inventories can be considered as negligible.

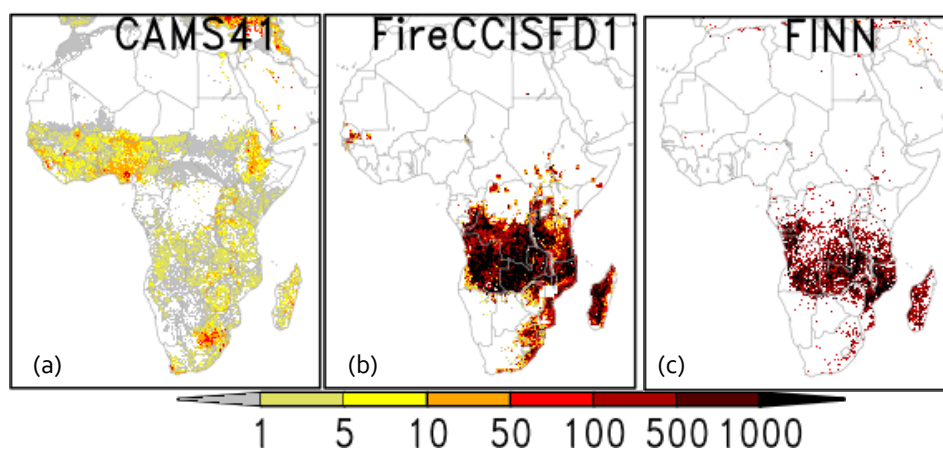


**Figure 3:** Burned area in September 2016 (in ha per 0.1° grid) (a) agricultural waste burning in CAMS41 based on agricultural statistics and (b) and (c) vegetation fires detected from satellites (FireCCISFD11: Sentinel-2A burn scar detection; FINN: MODIS active fire).

We applied the prep-chem-src1.0 pre-processor (Freitas et al., 2011) upon the monthly CAMS41 emission fields. The pre-processor creates hourly wrfchemi emission input fields, which, however, contain no diurnal cycle. Many anthropogenic emission sectors have a strong diurnal cycle, and representing this cycle is essential for simulating surface ozone chemistry (Bennet and Engardt, 2008). We therefore modified the wrfchemi emission input by applying the sector-wise diurnal cycles prescribed in Guevara et al. (2019). wrfchemi emission input to WRF-Chem are provided in UTC time. Since the WRF-Chem model domain covers several time zones, we explicitly introduced the diurnal cycles in correspondence to the local standard time.

#### 4. Fire emission inventories used in this study

The focus of this study is to construct and compare different fire emission estimates for Africa and to assess the impact of fire emission inventory uncertainties on atmospheric concentrations modelled by WRF-Chem. We perform WRF-Chem sensitivity simulations with three fire emission inventories:

- firstly, with FINNv1.5, which is a fire emission inventory specifically designed for WRF-Chem simulations and which is the default fire emission input used in WRF-Chem. For this reason, we consider WRF-Chem simulation with FINNv1.5 fire emission input, created with the standard FINNv1.5 pre-processor, as the reference run.
- secondly, with GFED4s, which is a general purpose fire emission inventory and which is the most widely used inventory in various regional to global climate and atmospheric chemistry applications. Because there is none publically available, we had to construct a pre-processor that converts GFED4s emissions into the required WRF-Chem fire emission input format.
- thirdly, with a new fire emission inventory that was constructed from scratch building upon FireCCISFD11 burned area information. Details on the methodology emission inventory are given in Section 4.3.

 <b>fire</b> cci	<b>Fire_cci</b>		Ref.	Fire_cci_D5.1_CAR_v2.1		
	<b>Climate Assessment Report</b>		Issue	2.1	Date	16/11/2020
					Page	15

#### 4.1. FINN

FINN is a global fire emission inventory that has been specifically designed to meet the requirements for a usage in regional atmospheric chemistry and air pollution modelling (Wiedinmyer et al., 2011). These applications optimally require hourly fire information at high spatial resolution (~10 km and higher), and, when used in air quality forecasting, also a near-real-time availability (Heil, 2019).

The latest FINN version, FINNv1.5, relies on MODIS MCD14DL C5 active fire counts. Burned area is indirectly estimated: an active fire detected in savanna and grassland or croplands is translated into an area burned of 0.75 km<sup>2</sup>, all other active fires into 1 km<sup>2</sup> burned. The burned area estimate is lowered proportional to the bare area fraction. MODIS C5 land cover information provides spatial information on fuel types. For this purpose, the individual land cover types are aggregated into six generic fuel type classes that are consistent with those used in the fuel load and emission factors databases of Akagi et al. (2011). FINNv1.5 is provided as ASCII files that list the time and coordinates of each detected fire, the fuel type and the estimated burned area and emission fluxes.

FINN is the most widely and evaluated fire emission inventory used in regional WRF-Chem atmospheric modelling applications. The main reason is that, up until very recently, FINN was the only fire emission inventory for which a well-tested pre-processor exists that creates fire emission input as required by WRF-Chem. Pre-processing emission input data for WRF-Chem from scratch is non-trivial and computationally demanding which is why WRF-Chem users limit their choice to FINN as fire emission input.

Yet, burned area estimated by the FINN method is highly uncertain. The underlying MODIS active fire product does not detect fires below ~100 ha. Cloud cover, and – in the case of understory fires – the tree canopy, and the satellite overpass timing additionally prevent fire detection

In this study, we downloaded FINNv1.5 emissions with MOZART4 chemical speciation from <http://bai.acom.ucar.edu/Data/fire/> (accessed on October 2020). We used the FINN fire\_emis WRF-Chem pre-processing utility downloadable from the same site to create hourly WRF gridded fire emission files from the original FINN data. For each trace species, the utility first calculates daily total emissions for each WRF grid cell, and then applies a default diurnal cycle to distribute them to hourly emission fluxes. The FINN fire\_emis utility also creates daily gridded fire size information, which is required for calculating the plume rise and hence the effective height at which the emissions are released into the atmosphere. In the gridding, the burned areas of all active fires that fall in the given grid and daily window are summed up. A maximum fire size of 2 km<sup>2</sup> (200 ha) in the gridded output is prescribed as default. The final fire size is then partitioned into fire sizes by fuel types. For this, a static map is used that covers four aggregated fuel type classes required for the plume rise calculation, namely grassland, savanna, tropical forest and extratropical forest.

#### 4.2. GFED4s

The Global Fire Emission Database (GFED) is a burned area and fire emission inventory that is most widely used in various climate and atmospheric chemistry applications. GFED combines burned area observations from the MODIS satellite sensor with a biogeochemical model to calculate fuel loads and combustion completeness at a monthly time step. The latest GFED version, GFED4s, builds upon the 500 m MCD64A1 C5 MODIS burned area product. To address the limitations of the MODIS sensor in resolving

 <b>fire</b> cci	<b>Fire_cci</b>		Ref.	Fire_cci_D5.1_CAR_v2.1		
	<b>Climate Assessment Report</b>		Issue	2.1	Date	16/11/2020
					Page	16

burned area from small fires, an indirect small fire estimate based on scaled MODIS active fire observations is added (Randerson et al., 2012; van der Werf et al., 2017). This 'small fire boost' increases the area burned in Africa by around 30% when compared to MCD64A1 C5 burned area.

In this study, we downloaded GFED4s emissions from <https://www.geo.vu.nl/~gwerf/GFED/GFED4/> (accessed on October 2020). GFED4s is delivered as annual hdf5 files that contain monthly, 0.25° gridded information on burned area and fire carbon and dry matter emissions. Additional data layers provide information on the fractional contribution of different fire types and on how to distribute monthly emissions over the days as well as the diurnal cycle. From these layers, when combined with recommended fire type-specific emission factors, we computed hourly, 0.25° degree gridded GFED4s fire emissions of various trace species for use as input in WRF-Chem. The recommended emission factors mostly base on (Akagi et al., 2011) and are provided at <https://www.geo.vu.nl/~gwerf/GFED/GFED4/ancill/> (accessed on October 2020). Species not contained in this compilation, but required by WRF-Chem are complemented as detailed in Table 3.

WRF-Chem requires curvilinearly gridded fire emission input data and additional data layers on fire size distribution and fuel type. For the remapping, we used a mass-conserving remapping scheme (Jones, 1999) discussed in more detail in Section 4.4.

For the required fractional fuel type layers, we use the layers computed by the FINN pre-processor (see Section 4.1). To compute fire size distribution, we sum up the total daily burned area falling within each curvilinear grid, and, similar to the FINN approach, we constrain a maximum fire size of 2 km<sup>2</sup>.

### 4.3. FireCCISFD11-derived fire emissions

FireCCISFD11 is a high resolution burned area product for sub-Saharan Africa for the year 2016. It has been produced from Sentinel-2 data at a spatial resolution of 20 m (Roteta et al., 2019). The acronym FireCCISFD11 stands for Fire\_cci Small Fire Dataset version 1.1, since the product was specifically developed to include burned areas from small fires (< 100 ha), which are omitted in currently existing coarse spatial-resolution burned area products (see Section 4.2).

The standard bottom-up approach to estimate fire emissions from burned area implies, firstly, multiplying burned area with estimates of the amount of fuel consumed per unit area burned fuel consumption and, secondly, multiplying the resulting product by emission factors (Seiler and Crutzen, 1980). Dependent upon the biome, the steps involve varying levels of stratification by vegetation types.

We use this approach to construct, in a first step, monthly 0.25° gridded fire emission estimates based upon the 0.25° gridded monthly FireCCISFD11 burned area. In a second step, we apply a pre-processor that converts the emission into hourly curvilinear fire emission data so that they can be ingested by WRF-Chem. Figure 4 provides a general overview of how FireCCISFD11 fire emissions were constructed. The construction involves the following key steps:

First, at a 0.25° monthly resolution, Fire\_cci burned area information (here: FireCCISFD11 product) is multiplied with GFED4s estimates of fuel consumption (see Section 4.3.1). The operation yields the total amount of dry biomass consumed by fires per month and grid cell.

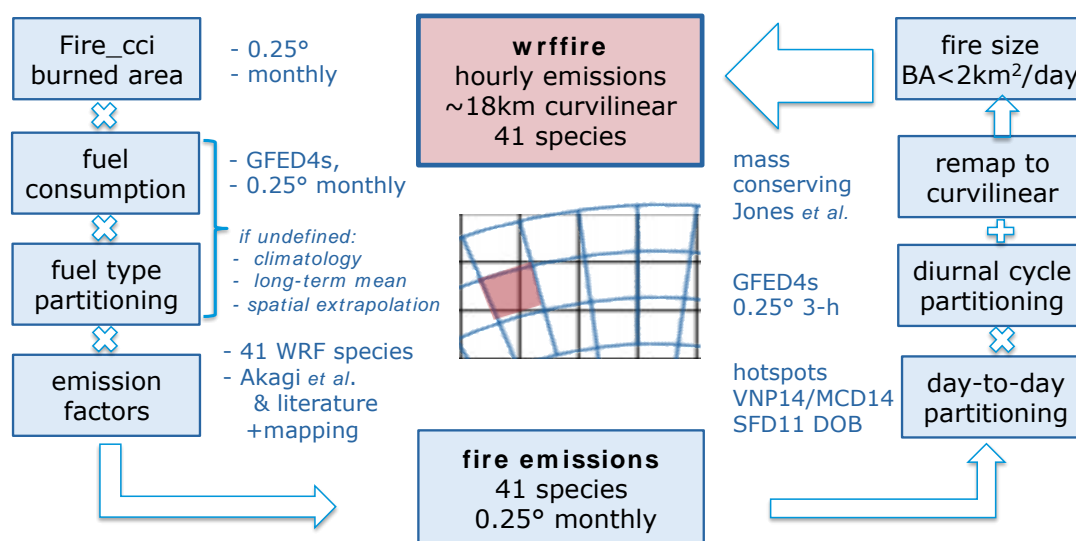


**Figure 4:** Flowchart illustrating how fire emissions are constructed from the gridded FireCCI5D11 burned area product and how they are pre-processed to comply with the specifications of WRF-Chem fire emission input data.

Second, the estimated total dry biomass consumed is split by fuel type using the 0.25° gridded monthly fuel type partitioning layer provided with the GFED4s product (see Section 4.3.2). The estimated total dry biomass consumed in each fuel type is then multiplied by fuel-type specific emission factors. The emission factors quantify the emitted mass of a given trace species relative to the dry biomass consumed by a fire (see Section 4.3.3). This operation, after summing over all fuel types, yields the estimated mass of a given trace species that is emitted by fires per 0.25° grid and month. For the WRF-Chem setup used in this study, emissions of 41 individual trace species were calculated.

Third, the monthly emission estimates are downscaled into daily (see Section 4.4.1) and then hourly emission estimates (see Section 4.4.2). For downscaling to daily emissions, we primarily used temporal information from the VNP14IMG and MCD14ML active fire products. For downscaling to hourly emissions, we used the diurnal cycle partitioning layer provided with the GFED4s product.

Fourth, the hourly, 0.25° gridded fire emissions are remapped to the curvilinear grid of the WRF-Chem model. For this, the mass conserving remapping approach is applied (see Section 4.4.3).

Fifth, a fire size data layer is added since it is required for plume rise calculation in WRF-Chem. To create this layer, we estimated daily area burned in each WRF-Chem model grid (see Section 4.4.4). To avoid excessive plume rise, we constrain maximum fire size to 2 km<sup>2</sup> per day.

In the following sections, we describe the details of the parameterisations used.

#### 4.3.1. Fuel consumption

Fuel consumption (FC) is the amount of biomass or fuel consumed per unit area burned. Fuel consumption largely depends on the vegetation type and the actual fuel moisture conditions during the burn (van Leeuwen et al., 2014). Fuel consumption can be estimated via three approaches:

- i. One is to upscale point field measurements to the whole study domain. For this, the measurement data are grouped by main land cover type, and the arithmetic mean for the individual types is then combined with spatial information on the land cover type distribution. The observational fundament for using field measurements to estimate fire emissions for Africa is, however, not robust. For example, the van Leeuwen et al. (2014) database of fuel consumption measurements contains no data for tropical forest or cropland fires in Africa, and there are only measurements from 3 and 5 sites, respectively, for woody and grassland savanna fires. Any extrapolation from these relatively few field measurements that, in addition, are not randomly distributed in time and space, to continent-wide average values involves a high risk of bias.
- ii. The other approach is to model fuel consumption with a fire-enabled dynamic vegetation model. The most well-known and state-of-the-art example for this is the GFED-CASA model, from which the GFED4s fuel consumption and fire emission inventory is created (van der Werf et al., 2017).
- iii. The third approach is the estimation of fuel consumption from satellite measurements of the radiant energy flux or "fire radiative power" (FRP) in combination with
  - a) fuel-type specific conversion factors, calculated from scaling FRP to GFED fuel consumption estimates (Kaiser et al., 2012), or
  - b) satellite measurements of aerosol optical depth (AOD) to quantify the relation between the emitted aerosol mass and FRP. With fuel-type specific aerosol emission factors, fuel consumption can then be calculated back.

To calculate fire emissions from FireCCISFD11 burned area, we take advantage of the fuel consumption rate estimates that are provided with the GFED4s database. GFED4s fuel consumption is calculated by dividing GFED4s dry matter combustion rates with GFED4s burned area rates. From this, we create 0.25° gridded fuel consumption maps for the months July to September (JAS) 2016 which we then multiply with FireCCISFD11 burned area information of the same months. To avoid multiplication of FireCCISFD11 burned area by zero in cases where GFED4s has no fire activity and hence no fuel consumption estimates, we first complement undefined values in the monthly GFED4s fuel consumption layer by the GFED4s JAS fuel consumption 2003–2016 climatology, then the remaining undefined values by the GFED4s 2003–2016 average fuel consumption, and as a last step, we perform spatial extrapolation. This approach aims at incorporating, as much as possible, the GFED4s temporal variability of fuel consumption, while maintaining a spatial pattern that is consistent with GFED4s fuel load distribution. Figure 5a illustrates the so-derived GFED4s fuel consumption layer for July 2016. Temporal variability in fuel consumption is particularly relevant in deforestation fires. Figure 5b and c display mean JAS 2016 fuel consumption together with the relative maximum deviation in the individual months from this mean. In 75% of all cases, the maximum deviation relative to the JAS average stays within 13%. Deviations are larger in deforestation fires, but, with few exceptions, stay within 50%.

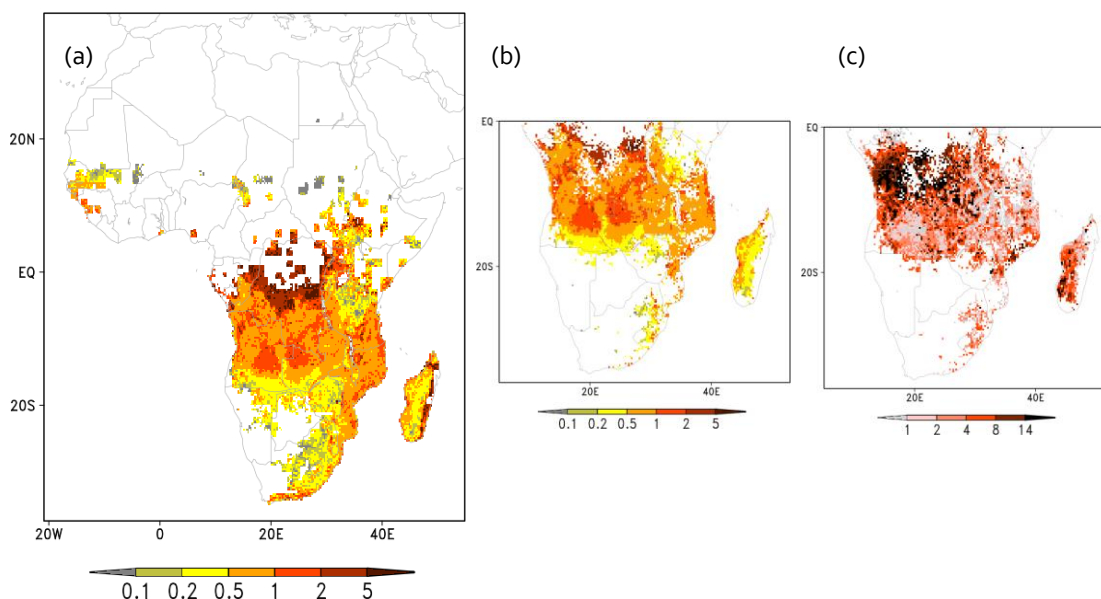


**Figure 5:** (a) GFED4s-based fuel consumption layer for the study domain for July 2016 (kg fuel per m<sup>2</sup> burned). Only shown are grid cells with non-zero fire activity in the FireCCISFD11 July data. (b) JAS 2016 mean GFED4s fuel consumption across southern hemispheric Africa (in kg fuel per m<sup>2</sup> burned). Only shown are grid cells where GFED4s exhibits fire activity in all three months. (c) Absolute deviation of GFED4s monthly fuel consumption from the July to September mean (in %). The colour levels correspond to the 10, 25, 50, 75 and 90 field percentiles.

#### 4.3.2. Fuel type stratification

Land cover information of the area burned is essential for calculating fire emissions since the land cover type indicates what kinds of fuels are being combusted. Fire emission factors depend on fuel type (Akagi et al., 2011; Andreae, 2019). The Akagi et al. (2011) emission factor compilation provides fuel-type average emission factors for savanna, forest (differentiated into tropical, temperate and boreal), peat, and cropland burning. The emission factors for tropical forest are representative for fires in areas with high canopy coverage, while the emission factors for savanna apply for fires that occur in grasslands with scattered trees or scrubs (Akagi et al., 2011). An equivalent fuel-type classification is also inherent to the Andreae (2019) compilation of emission factors. Furthermore, the database of fuel consumption field measurements by van Leeuwen et al. (2014) uses a similar fuel type classification.

The fuel types used in the fuel partitioning layer that is provided with the GFED4s database are consistent with the above-mentioned classification. The layer is computed from the MODIS MCD12C1 land cover type product (Friedl et al., 2010) and quantifies the fractional contribution of individual fuel types to the total fuel consumption within each 0.25° grid cell and month. We use the GFED4s fuel partitioning layers, which we spatially extrapolated in the same way as the GFED4s fuel consumption layer (see section 4.3.1), to apply fuel-type specific emission factors on the FireCCISFD11-derived fuel consumption estimates.

Using the GFED4s fuel type partitioning, roughly 92% of the total biomass burned across JAS 2016 in the continental Africa study domain are treated as savanna fires, around 7% as agricultural fires, and only 0.7% as deforestation fires (Figure 6).

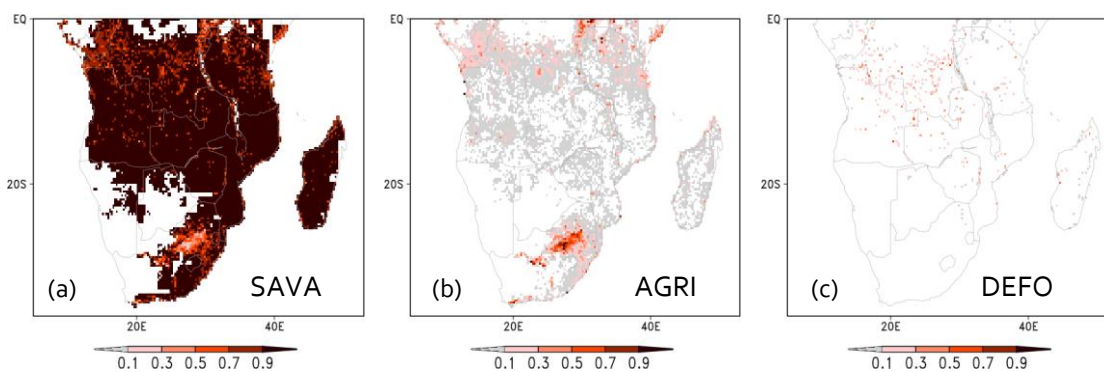


**Figure 6:** (a-c) GFED4s-based fuel type partitioning layer for the southern hemispheric regions of the study domain (JAS 2016 mean) expressing the fractional contribution of fuel types to total fuel consumption. Shown are grid cells where the FireCCISFD11 product records fire activity in JAS 2016. SAVA, AGRI and DEFO stands for savanna, agriculture, deforestation fires, respectively.

### 4.3.3. Emission factors

Emission factors quantify the emissions of trace species or aerosols per amount dry biomass consumed by the fire. There are two landmark compilations of biomass burning emission factors. One is the (Andreae and Merlet, 2001) compilation with its recent update (Andreae, 2019), the other is the (Akagi et al., 2011) compilation. Both provide best estimate emission factors for a large variety of air pollutants, classified by main fuel types. While both are comprehensive literature reviews of published emission factor measurements, they differ in terms of to what degree results from field versus laboratory measurements are included and in terms of fuel type classification. For most emitted species, FINN and GFED4s use values from Akagi et al. (2011). Emission factors missing in Akagi et al. (2011) are complemented with Andreae and Merlet (2001) and other sources. To calculate emissions from FireCCISFD11 burned area information, we use the same emission factor parameterisation as those recommended for GFED4s (Table 3). Emission factors for species required by WRF-Chem, but not provided by GFED4s, are complemented from various sources.

While for most species, FINN and GFED4s use largely similar emission factors, there are drastic differences for some individual species, such as in the case of NO<sub>x</sub>. In addition, FINN uses separate emission factors for grassland savanna and woody savanna, but it remains unclear from where these values are taken. In contrast, GFED4s only uses a single emission factor for savanna fires. The NO<sub>x</sub> emission factors used in FINN for the different fuel types, calculated as the sum of the NO and NO<sub>2</sub> emission factors, differ substantially from the Akagi et al. (2011) compilation that is used in GFED4s and that we also apply in FireCCISFD11. FINN NO<sub>x</sub> emissions per unit mass fuel burned in grassland and woodland savannas are 28% to 41% lower than in GFED4s. In contrast, in tropical forest and croplands FINN NO<sub>x</sub> emissions are distinctively higher (28% – 36%) (Table 4). Additionally, FINN and GFED4s resp. FireCCISFD11 use different fuel type maps and classifications, resulting in substantial differences in overall fire emission estimates that are solely attributable to the emission factor parameterisation.

The choice of the emission factors and fuel type maps also largely control the differences between GFED4s, FireCCISFD11, FINN and other fire emission inventories such as GFAS, QFED and FEER (Table 4). For example, the NO<sub>x</sub> emission factor used for savanna in GFAS is 50% lower than the factor used in GFED4s and FireCCISFD11. And, most strikingly, the BC emission factor used in QFED for tropical forest is by a factor of 6.7 to 7.6 larger than in any other fire inventory, and the factor used for savanna is by a

factor of 1.6 to 2.3 larger. Hence, the differences between different fire emission inventories that are due to the choice of the emission factors can be in the same magnitude, or even bigger, than the differences that are caused by the choice of the underlying burned area product.

**Table 3:** Emission factors used to calculate FireCCISFD11 fire emissions (in g per kg dry matter burned). 'tracer' identifies to which WRF-Chem tracers the species is mapped.

species	tracer	SAVA	BORF	TEMF	DEFO	AGRI
CO	co	63.00	127.00	88.00	93.00	102.00
OC	oc	2.62	9.60	9.60	4.71	2.30
BC	bc	0.37	0.50	0.50	0.52	0.75
SO2	so2	0.48	1.10	1.10	0.40	0.40
C2H6	c2h6	0.66	1.79	0.63	0.71	0.91
CH3OH	ch3oh	1.18	2.82	1.74	2.43	3.29
C2H5OH	c2h5oh	0.02	0.06	0.10	0.04	0.04
C3H8	c3h8	0.10	0.44	0.22	0.13	0.28
C2H2	c2h2	0.24	0.18	0.26	0.44	0.27
C2H4	c2h4	0.82	1.42	1.17	1.06	1.46
C3H6	c3h6	0.79	1.13	0.61	0.64	0.68
C5H8	isop	0.04	0.15	0.10	0.13	0.38
C10H16	apin	0.08	2.00	2.00	0.15	0.01
C7H8	toluene	0.08	0.48	0.19	0.26	0.19
C6H6	benzene	0.20	1.11	0.27	0.39	0.15
C8H10	xylenes	0.01	0.18	0.13	0.11	0.11
Higher_Alkenes	bigene	0.13	0.38	0.37	0.27	0.33
Higher_Alkanes	bigalk	0.05	0.35	0.22	0.07	0.34
CH2O	ch2o	0.73	1.86	2.09	1.73	2.08
C2H4O	ch3cho	0.57	0.77	0.77	1.55	1.24
C3H6O	ch3coch3	0.16	0.75	0.54	0.63	0.45
NH3	nh3	0.52	2.72	0.84	1.33	2.17
HCN	hcn	0.41	1.52	0.72	0.42	0.29
HCOOH	hcooh	0.21	0.57	0.28	0.79	1.00
CH3COOH	ch3cooh	3.55	4.41	2.13	3.05	5.59
MEK	mek	0.18	0.22	0.13	0.50	0.90
CH3COCHO	mgly	0.73	0.73	0.73	0.73	0.73
HOCH2CHO	glyald	0.25	0.86	0.86	0.74	0.71
C7H8OH	gres	0.46	0.67	0.67	0.46	0.41
C3H6O2	acetol	0.56	2.11	1.13	1.81	3.12
C4H6O	macr	0.10	0.11	0.14	0.15	0.28
C4H6O	mvk	0.23	0.10	0.17	0.39	0.48
CH3CN	ch3cn	0.17	0.31	0.22	0.49	0.25
C10H16	c10h16	0.00	0.00	0.00	0.00	0.00
NO (as NO)	no	2.93	0.68	1.44	1.91	2.33
NO2(as NO2)	no2	1.49	0.34	0.74	0.98	1.19
C5H6O2	open	1.58	0.33	0.33	0.29	1.58
PMsulfate	sulf	0.20	0.36	0.28	0.23	0.17
PM2.5c	pm25	4.12	5.12	2.76	3.81	3.16
PM10c	pm10	1.66	3.54	2.98	2.10	1.45

Note: If not noted otherwise, emission factors are similar to those recommended for GFED4s ([https://www.geo.vu.nl/~gwerf/GFED/GFED4/ancill/GFED4\\_Emission\\_Factors.xlsx](https://www.geo.vu.nl/~gwerf/GFED/GFED4/ancill/GFED4_Emission_Factors.xlsx), last accessed August 3, 2020).

<sup>a</sup> data source: (Koss et al., 2018). BORF&TEMF=average EF over all conifer fuels; AGRI=rice straw EF; PEAT=peat EF;SAVA&DEFO=average EF over all fuels. <sup>b</sup> data source: (Andreae, 2019). <sup>c</sup> (Emmons et al., 2020) defines this group as 'lumped monoterpenes, as  $\alpha$ -pinene'. According to (Akagi et al., 2011),  $\alpha$ -pinene fire emissions are only of relevance for boreal and extratropical forest fires; set to zero for a WRF simulation over Africa. <sup>d</sup> NO<sub>x</sub> split into NO and NO<sub>2</sub> based on G. Brasseur (pers. communication), see section 4.3.3 <sup>e</sup> data source: (Akagi et al., 2011). <sup>f</sup> PM<sub>2.5c</sub> is the PM<sub>2.5</sub> fraction excluding OC, BC, and sulphate data. PM<sub>10c</sub> is the PM<sub>10</sub> fraction excluding PM<sub>2.5</sub> and excluding sulphate in the PM<sub>10-2.5</sub> fraction.

**Table 4.** Emission factors for carbon monoxide (CO), oxides of nitrogen (NO<sub>x</sub>) and black carbon (BC) (in g per kg biomass burned) used in different fire emission inventories. N.B. FireCCISFD11 uses the GFED4s emission factors.

Inventory	CO			NO <sub>x</sub> <sup>h</sup>			BC		
	SAVA	TROF	AGRI	SAVA	TROF	AGRI	SAVA	TROF	AGRI
GFED4s <sup>a</sup>	63	93	102	3.9	2.6	3.1	0.4	0.52	0.75
FINNv1.5 <sup>b</sup>	59/68 <sup>g</sup>	92	111	2.8/2.3 <sup>g</sup>	3.3	4.2	0.37/0.50 <sup>g</sup>	0.52	0.69
GFASv1.2 <sup>c</sup>	61	101	92	2.1	2.3	2.3	0.46	0.57	0.42
QFED <sup>d</sup>	65	104	–	3.9	1.6	–	0.86	3.80	–
FEER <sup>e</sup>	67	100	105	2.6	2.6	2.7	0.48	0.56	0.46
Andreae19 <sup>f</sup>	69	104	76	2.5	2.8	2.40	0.53	0.51	0.42

*Note.* SAVA = savanna, TROF = tropical forest, AGRI = agricultural residues.

<sup>a</sup> GFED4s emission factors are primarily based on (Akagi et al., 2011).

<sup>b</sup> FINN emission factors generally base on a prototype version of (Akagi et al., 2011), complemented by various other sources. NO<sub>x</sub> emission factor is calculated as the sum of the NO and NO<sub>2</sub> emission factors used in FINN.

<sup>c</sup> GFAS emission factors base on (Andreae and Merlet, 2001) with updates from the literature through 2009.

<sup>d</sup> QFED emission factors generally base on (Andreae and Merlet, 2001). The source of the BC emission factors is unclear. Values given here are calculated back from the species-to-CO<sub>2</sub> emission ratios (QFED v2.5r1 year 2016 data for Africa) in combination with the (Andreae and Merlet, 2001) CO<sub>2</sub> emission factors.

<sup>e</sup> FEER emission factors are on (Andreae and Merlet, 2001), with updates provided by Andreae in 2014. Values given here are calculated back from the species-to-C emission ratios (FEERv1.0-G1.2 year 2016 data for Africa), assuming a dry matter carbon content of 50%.

<sup>f</sup> emission factors recommended by (Andreae, 2019).

<sup>g</sup> (GS/WS) FINN uses separate emission factors for grassland savanna (GS) and woody savanna (WS).

<sup>h</sup> NO<sub>x</sub> emission factor as NO, i.e. EF(NO<sub>x</sub>)=EF(NO)+EF(NO<sub>2</sub> as NO).

### *NO<sub>x</sub> emission parameterisation*

The WRF chemistry scheme represents NO<sub>x</sub> emissions as separate NO and NO<sub>2</sub> chemical tracers. Emission factors for oxides of nitrogen are generally provided as NO<sub>x</sub> though, and information is scarce on how to best split them into separate NO and NO<sub>2</sub> emissions. NO<sub>x</sub> are one of the main precursors of lower atmospheric ozone, and the ozone chemistry is sensitive to the NO and NO<sub>2</sub> emission split.

Primary NO<sub>x</sub> emissions from combustion sources are typically considered to consist of 90-95 vol-% NO and the remainder of NO<sub>2</sub> (Barten et al., 2020; Valencia et al., 2018). For biomass burning, other NO/NO<sub>x</sub> ratios are sometimes used, e.g. 85% (Castellanos et al., 2014) and 75% (Trentmann et al., 2003), in line with an average 80% NO/NO<sub>x</sub> ratio measured in combustion chamber experiments with various fuel types (Yokelson et al., 1996). In aged biomass burning plumes with quasi-photostationary state, a NO/NO<sub>x</sub> ratio of 25% is common (Mebust et al., 2011).

In the construction of the GFED4s and FireCCISFD11 WRF-Chem fire emission input, we segregate NO<sub>x</sub> fire emissions into NO and NO<sub>2</sub> using a molar split of 75% NO: 25% NO<sub>2</sub> (Guy Brasseur, personal communication, 18 June 2020). This NO/NO<sub>x</sub> split, however, differs strongly from the split used in FINNv1.5 which parameterises, e.g., NO<sub>x</sub> fire emissions in grassland savanna (GSAV), woody savanna (WSAV) and tropical forest

	<b>Fire_cci</b> <b>Climate Assessment Report</b>		Ref.	Fire_cci_D5.1_CAR_v2.1		
			Issue	2.1	Date	16/11/2020
			Page		23	

(TROF) with a NO/NO<sub>x</sub> ratio of 29%, 62% and 39%, respectively (see also (Wiedinmyer et al., 2011) Table 1).

#### *Aerosol emission parameterisation*

To estimate PM<sub>10</sub> fire emissions in the GFED4s and FireCCISFD11 inventories, we apply a factor of 1.25 on the PM<sub>2.5</sub> emission estimates. We are not using PM<sub>10</sub> emission factors from the Akagi et al. (2011) compilation because of inconsistencies in the particle emission factors, such as that e.g. for tropical forest, the average emission factor for total particulate matter is 30% lower than the PM<sub>10</sub> emission factor. Instead, we assume that PM<sub>2.5</sub> contributes 80% to the PM<sub>10</sub> mass emitted, which is in line with the average PM<sub>2.5</sub>/PM<sub>10</sub> measured across various fire types (Li et al., 2007; Stephens et al., 2007; Yokelson et al., 2008). We do not attribute BC or OC emissions to the coarse fraction of PM<sub>10</sub> (PM<sub>10-2.5</sub>) since their contribution is generally marginal (< ~1%) in fresh biomass burning aerosols; Aurela et al. (2016) show that this fraction contains less than 1%. This parameterisation also largely agrees with the PM<sub>2.5</sub>/PM<sub>10</sub> ratio used in FINNv1.5, except for tropical deforestation fires where FINN assumes a ratio of 0.5. The sulphate mass content in biomass burning aerosols is typically between 0.5% and 3% (Bi et al., 2019; Ferek et al., 1998); we here take a best guess estimate of 1.5% to parameterise sulphate emissions.

In the WRF-Chem simulation with FINN, we use the default WRF-Chem fire emission mapping scheme for aerosols. In this scheme, OC, BC, and sulphate emission input to the WRF model is scaled from PM<sub>2.5</sub> and PM<sub>10</sub> emissions. For example, OC fire emission input to the WRF model is calculated as 'OC -> 0.24\*PM<sub>2.5</sub> + 0.3\*PM<sub>10</sub>', which implies that the OC contribution in the aerosol emissions is constant across vegetation types burned. In the WRF-Chem simulations with GFED4s and FireCCISFD11 fire emissions, we apply a mapping that uses explicit OC, BC, and sulphate fire emissions.

### **4.4. Pre-processing fire emission inputs for WRF-Chem**

There are several publications specifically dedicated to the pre-processing of emission inventories for use in WRF-Chem. Fire emission pre-processors have been developed and tested for FINN (Wiedinmyer et al., 2011) and GFAS (Guevara et al., 2019; Pino-Cortés et al., 2020). Pre-processors for anthropogenic emission inventories have been developed by Freitas et al. (2011), Guevara et al. (2019), Schuch et al. (2019) and Vara-Vela et al. (2016). One challenge in creating these pre-processors is to achieve mass-conserving spatial interpolation of emission input data to the WRF model grid and to map emissions of individual trace species to WRF-Chem tracers. No pre-processor for fire emissions from gridded burned area products has been published in literature or open-source code platforms. For this reason, a pre-processor was developed from scratch that provides WRF-Chem fire emission input data from GFED4s and FireCCISFD11.

#### **4.4.1. Diurnal cycle**

By default, FINN first computes daily aggregated fire emissions and then redistributes them to hourly emission fluxes using a single diurnal profile. In this profile, fire emission flux is highest at noon – 57% of the daily emissions are released between 12am and 3pm – while emission intensity is minimal between 7pm to 8am.

The monthly GFED4s product contains a data layer with scalars enabling users to calculate 3-hourly emission fluxes. Constructed and extrapolated from GOES WF\_ABBA observations by Mu et al. (2011), the scalars describe climatological mean

diurnal cycles of fire activity. For continental Africa, GFED4s and FINN assume a largely similar diurnal cycle (Figure 7). The GFED4s diurnal scalars are defined for entire continental Africa and are being used to construct the diurnal cycle of the FireCCISFD11 fire emissions.

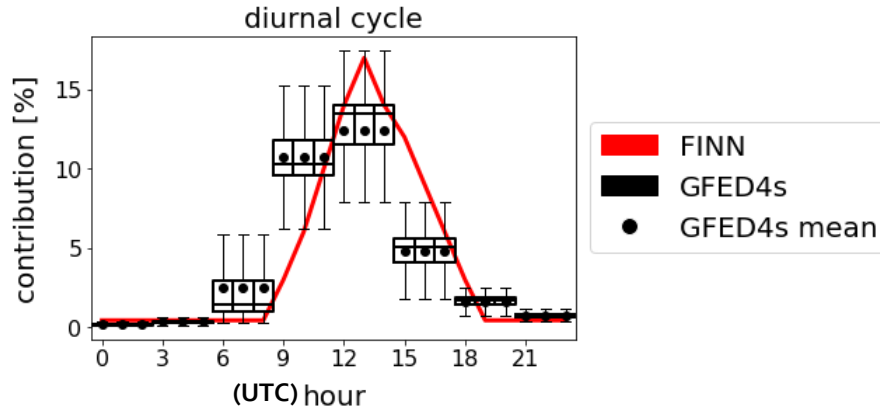


**Figure 7:** Parameterization of the diurnal emission profile in FINN and GFED4s. The GFED4s profile is extracted from the 3-hourly GFED4s diurnal\_cycle data layer for July 2016. Only data points with active fires in the WRF-Africa model domain are included. The boxplots reflect the diurnal cycle variability within this domain, the mean GFED4s diurnal cycle profile is indicated by a black dot. The FINN diurnal profile is extracted from the fire\_emis preprocessor.

Also Zhang et al. (2014) uses the temporal scalars developed by Mu et al. (2011) to distribute monthly or daily fire emission inventories into hourly emission fields for use in WRF-Chem.

#### 4.4.2. Day-to-day variability

To distribute monthly FireCCISFD11 burned area into daily burned area, we use temporal fire activity information from two products: (a) S-NPP VIIRS 375 m (VNP14IMG) and (b) collection 6 (C6) MODIS 1 km (MCD14ML). From these, we calculate the total number of daily fire counts per  $0.25^\circ$  grid and then apply the ratio of the daily to monthly total fire counts as scalar to downscale monthly FireCCISFD11 burned area into daily time steps. Only active fire observations classified as presumed vegetation fire are included. We use a combination of two active fire products to maximise the overlap with FireCCISFD11 burned area. Yet, only 82.4% of all FireCCISFD11 grid cells with nonzero monthly burned area show fire activity in the combined VIIRS-MODIS product across July to September 2016, indicating that FireCCISFD11 has a higher fire detection rate as these two active fire products combined. The overlap of the MODIS active fire product alone is 71.4% and that of the VIIRS product 81.5%. VIIRS, thanks to its finer spatial resolution, is capable of detecting fires of smaller size and lower intensity (Fu et al., 2020; Li et al., 2020). Reversely, only 0.5% of the grid cells in the combined VIIRS-MODIS product have no corresponding monthly FireCCISFD11 burned area signal. These active fire observations missed by FireCCISFD11 largely coincide with observational gaps (see (Figure 8a-c).

Burned areas in FireCCISFD11 grid cells with no corresponding active fire signal are small and scattered across Sub-Saharan Africa. Their median size is 74 ha (per  $0.25^\circ$  grid and month) compared to 3111 ha in the grid cells with corresponding active fire signal. Because the fires are small, they contribute only 1% to the total FireCCISFD11 area burned across July to September 2016. To downscale these monthly FireCCISFD11

burned area observations into daily time resolution, we create daily  $0.25^\circ$  gridded burned area estimates from the day of burn layer contained in the FireCCISFD11 pixel product, and then use the daily contribution to monthly burned area as scaling matrix. The FireCCISFD11 product builds on imagery from the Sentinel-2A satellite, which has a revisit time of 10 days at the Equator (Roteta et al., 2019). Occasionally, the effective image frequency is lower due to technical acquisition or archiving problems or due to cloud coverage. The low temporal sampling implies that burn scars are frequently detected only days or weeks after the fire has actually taken place (Figure 8d). Due to these restrictions, the date of the burned pixel provided with the FireCCISFD11 pixel product may not be coincident with the actual burning date. In fact, the specified burn date may correspond to a date that lags up to weeks behind the actual burn date, particularly in areas with high cloud coverage. For this reason, the date of burn information provided in the FireCCISFD11 pixel product cannot be considered as the first choice to create scalars for distributing monthly burned area into daily time steps, and we use it only when more accurate time information from active fire observations is missing.

Figure 8 (a-c) displays the observational coverage at which the FireCCISFD11 product has been produced. Most regions across Sub-Saharan Africa have full observational coverage across July to September 2016. Cloud contamination and other observational difficulties substantially decrease the coverage across countries bordering the Gulf of Guinea, notably in September 2016 (Figure 8c), and, because the observational gaps occur in the proximity of widespread fires (Figure 8d), it is likely that they entail substantial underestimation of burned surfaces.

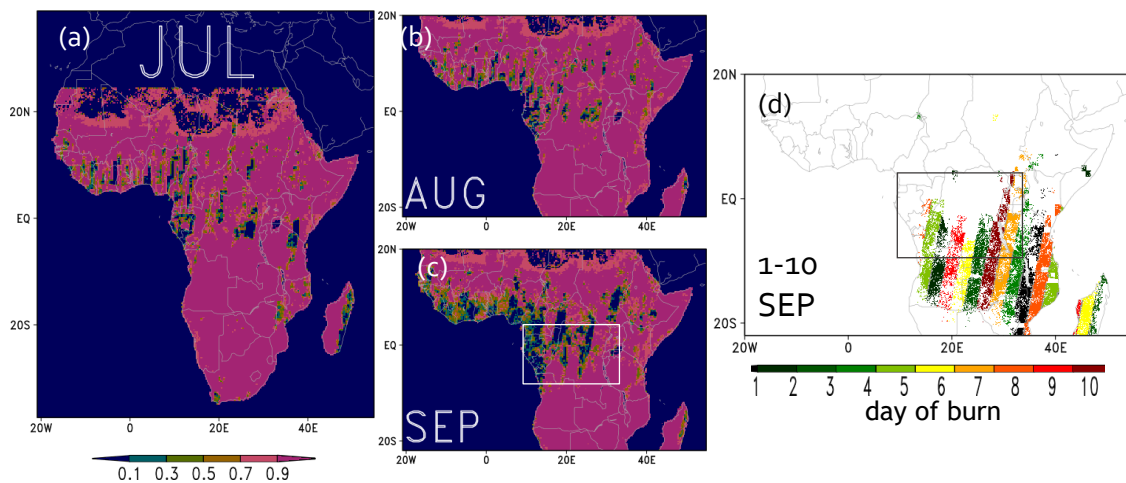


**Figure 8:** (a-c) Observational coverage in the FireCCISFD11 product during July to September 2016, expressed as fraction of the burnable area within each  $0.25^\circ$  grid cell for which valid satellite observations were available. The FireCCISFD11 product covers continental Africa south of  $25^\circ$  N. Low observational coverage between  $15^\circ$  and  $25^\circ$  N is related to the presence of unburnable land cover. (d) Day of burn computed from the FireCCISFD11 pixel product for the period 1<sup>st</sup> – 10<sup>th</sup> September 2016. The coloured bands reflect the 290 km swath width of the MSI-L1C sensor. Rectangles in (c) and (d) highlight observational gaps occurring in the proximity of fires.

#### 4.4.3. Remapping to the curvilinear model grid

One component of the pre-processor is the remapping of emissions to the curvilinear WRF grid. In our study, this implies remapping  $0.25^\circ$  data to a WRF curvilinear grid with a spatial resolution of roughly 18 km. Bilinear spatial interpolation is the most commonly used method to interpolate input data to model grids because it is easy to implement and it has low computational demands (Kim et al., 2019). However, this interpolation does not preserve the integrals of the data. Figure 9 illustrates that bilinear interpolation of

0.25° gridded burned area data to the WRF curvilinear grid increases the domain-integrated burned area by 28%. Nearest neighbour remapping leads to comparable deviations. Both remapping schemes are therefore unsuitable for pre-processing fire emission input. We therefore implemented an integral-preserving first order conservative remapping scheme (Jones, 1999) in which the weight of a source cell is proportional to area of the source cell intersected by target cell. Figure 9 and Figure 10 show that that conservative remapping of the 0.25° gridded burned area data to the curvilinear WRF grid conserves the domain integrals, and leads to, aside from unavoidable random interpolation errors, largely similar results when compared to remapping to the curvilinear grid directly from the pixel product.

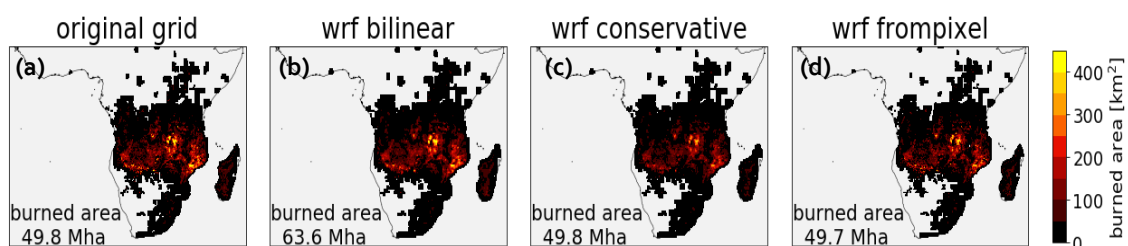


**Figure 9:** FirecciSFD11 burned area in September 2016 (a) original 0.25° grid product and (b)-(c) original grid product interpolated to the WRF-Chem grid with bilinear and conservative remapping, respectively, and (d) pixel product interpolated to WRF-Chem grid (with conservative remapping). Number show total burned area across Sub-Saharan Africa.

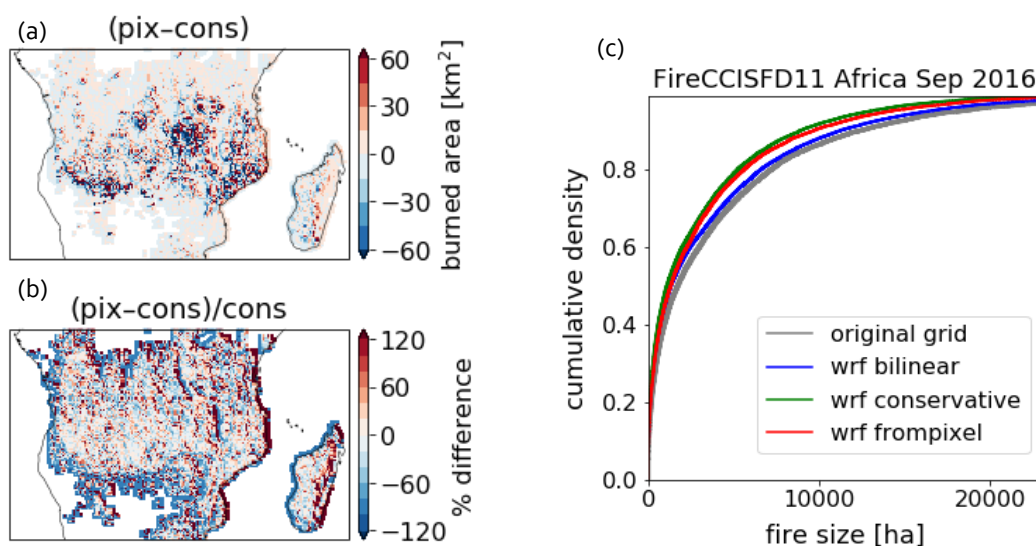


**Figure 10:** (a) Absolute and (b) relative difference between FireCCISFD11 burned area mapped to the WRF-Chem curvilinear grid from the pixel product ("pix", see also **Figure 9c**) and from the grid product ("cons", see also see also **Figure 9d**). (c) Gridded fire size distribution (i.e. burned area per grid and month) in the different remapping schemes (see also **Figure 9**).

#### 4.4.4. Fire size distribution for WRF-Chem plume rise calculation

WRF's plume rise module that calculates the injection height of fire emissions requires the availability of a fire size variable (FIRESIZE\_AG\*) in the WRF-CHEM fire emission input data (wrffirechemi\*). The FINN preprocessor computes this variable from active fire count information; however, this methodology is not applicable when creating WRF emission input data from gridded burned area products.

We explored the option to make use of the monthly number of burn patches (NoP) layer provided with the gridded Fire\_cci burned area products. Theoretically, the burned area

to NoP quotient could contain an indicator of the mean fire size. However, the analysis of the layers revealed unrealistic values when compared to e.g. the FRY fire patch database (Laurent et al., 2018) or the number of fires identified in the Global Fire Atlas (GFA, Andela et al., 2019), pointing to an error in the computation of this layer. For example, the FireCCISFD11 NoP layer identifies 24 million individual burned patches in July 2016 across Africa. In FRY or GFA, the number of identified patches ranges from 21 to 71 thousands (Table 5). Also, there is a factor of 10 difference when comparing the FireCCI51 NoP with the number identified in the FRY MCD64C6 product, despite both using a comparable temporal cut-off of around 15 days. The FireCCISFD11 burned area estimate, when divided by the NoP information, would correspond to an average fire size of 2 ha, which is unrealistically low. While 2 ha is a typical size for agricultural fires set for clearing crop residues by smallholders (Shaffer, 2010), most fires in Africa are savanna fires and these are on average 500 ha in size (Andela et al., 2019). Using information from FRY or GFA instead is not considered as a viable option to derive the fire size variable in the WRF-CHEM fire emission input data since the required consistency with the fire emission data layer cannot be assured.

**Table 5:** Monthly total number of individual fires identified in Africa in different burned area products (in thousand).

	GFA MCD64C6	FRY MCD64C6	FireCCI51	FireCCISFD11
<i>cutoff (days)</i>	<i>4-10</i>	<i>14</i>	<i>15</i>	<i>15</i>
Jul-16	71	21	320	23,930
Aug-16	79	28	312	26,585
Sep-16	59	21	149	22,741

In the end, we used total daily burned area within each curvilinear grid as mean fire size proxy. Analogous to FINN, we apply an upper constraint of 2 km<sup>2</sup> per grid and day to prevent excessive plume rise in WRF-Chem. We partition mean fire size into the four fuel types that are required for the plume rise parameterisation using the static map provided with FINN (see also section 4.1). The cumulative density plots and the boxplots in Figure 11 - Figure 13 (a, b) show the fire size distribution provided to WRF-Chem by FINN, GFED4s and FireCCISFD11. Please note that we adopt here the mean fire size terminology used in FINN which refers to the daily area burned per WRF-Chem curvilinear grid, which, of course, is not equivalent to the mean fire size in the reality. The figures show the fire sizes after the partitioning into fuel classes and prior to it ("ALL"). The latter exhibits a bimodal behaviour in FINN with roughly 30% of all fires in the size range between 50 and 100 ha per grid and day and another 50% in the size range between 180 and 200 ha per grid and day. GFED4s and FireCCISFD11, in contrast, show a smooth increase in the cumulative distribution function starting from fire sizes close to 0 ha. The spike in the distribution at 200 ha per grid and day is the result of trimming the maximum fire size to this value, which affects 40% of all fire grid cells in FINN, but only 30% and 18% in FireCCISFD11 and GFED4s, respectively. Overall, mean fire size in FINN is considerably larger than in FireCCISFD11 or GFED4s (144 ha versus 101 and 69 ha, respectively (Figure 11 - Figure 13 (b)), implying that the injection heights of smoke plumes will, on average, be highest when using the FINN inventory. In the plume rise parameterisation, the majority of the burned surfaces will be treated as savanna fuels (52 – 56%), followed by grassland fuels (31 – 40%) (Figure 11 - Figure 13 (c)).

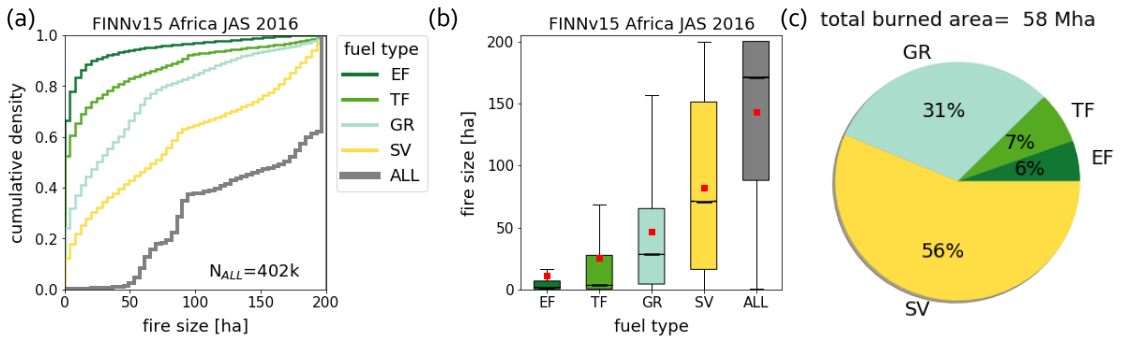


**Figure 11:** (a) Cumulative histogram of FINN mean hourly fire size per WRF grid for the individual fuel type classes (period July to September 2016). (b) Boxplots of mean fire size per WRF grid by fuel type. Red marker denotes the arithmetic mean size. (c) Contribution of FINN fuel types to total burned area calculated from the WRF mean fire size variable for the WRF-Chem Africa domain. The following abbreviations are used: EF=extratropical forest, TF=tropical forest, GR=grassland, SV=savanna. ALL is the total fire size per WRF (sum over the four fuel type classes).

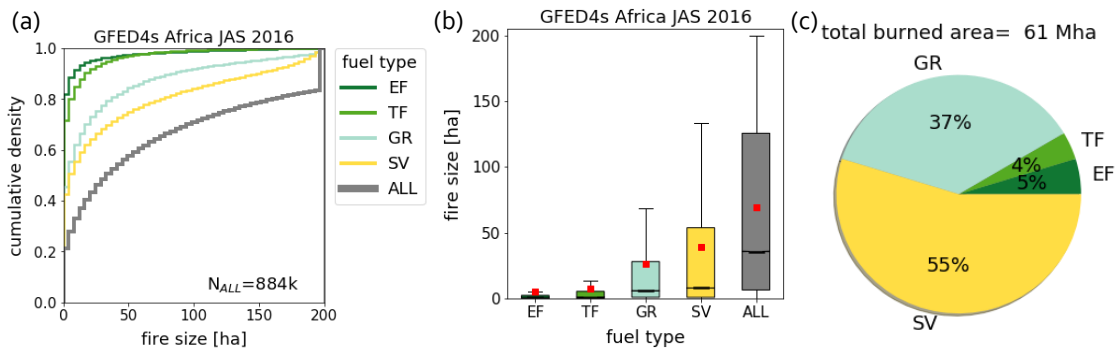


**Figure 12:** Same as Figure 11, but for GFED4s.

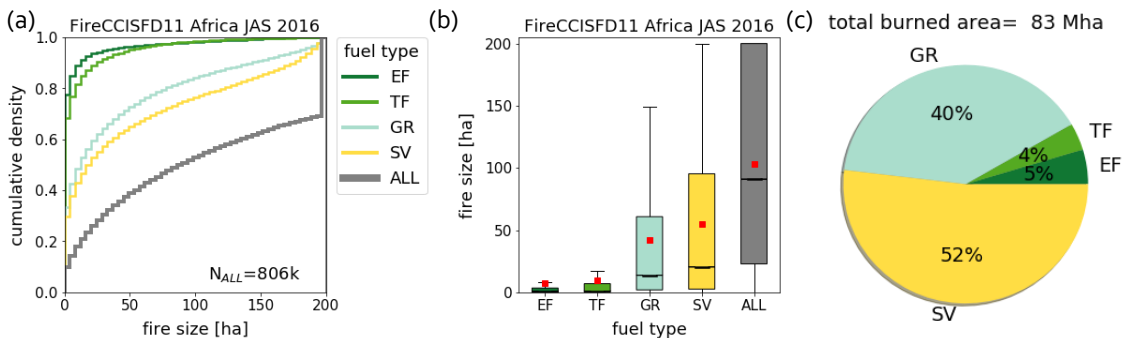


**Figure 13:** Same as Figure 11, but for FireCCISFD11.

Further evaluation is required to assess how differences in the fire size distribution influence plume rise calculation in WRF-Chem and how this affects modelled surface concentrations close and distant to the fire sources. There is no recommendation how to parameterise mean fire size when using fire emission inventories other than FINN. Looking at WRF-Chem studies that used custom fire emission inventories, we note that Saide et al. (2015) assumed a default fire size of 25 ha in their WRF-Chem simulation over the California, USA, with the FRP-based QFED fire emission inventory, while others do not specify what fire size parameterisation they used (e.g. Hodnebrog et al. (2012), Wang et al. (2018). Zhang et al. (2014)).

#### 4.5. Fire Emission Estimates for Africa

Table 6 summarises fire emission estimates for Africa for the period July to September 2016. In addition to the three 'bottom-up' fire emission inventories that we use in this study which rely on burned area estimates, we also include three FRP-based emission inventories for comparison (GFAS v1.3, FEER v1.0, QFED v2.5 FREM v2). Furthermore, we provide estimates from four anthropogenic emission inventories.

Emission inventories estimate that fires burning across Africa during July to September 2016 emitted in total between 35 to 102 Tg carbon monoxide (CO), 1.4 to 5.3 Tg oxides of nitrogen (NO<sub>x</sub>) and 0.32 to 0.85 Tg black carbon (BC) (Table 6). Fire emissions of CO are substantially larger than those emitted by anthropogenic sources. In most inventories included in this study, fire emissions of NO<sub>x</sub> and CO are also larger than those from anthropogenic sources.

**Table 6:** Total emissions of carbon monoxide (CO), oxides of nitrogen (NO<sub>x</sub>) and black carbon (BC) emitted from vegetation fires in Africa throughout July to September 2016 (in Tg), as estimated by various satellite-derived inventories. Estimates of anthropogenic emissions are shown for comparison.

Inventory	CO [Tg]	NO <sub>x</sub> [Tg] <sup>h</sup>	BC [Tg]
FireCCISFD11	89.9	5.2	0.53
FINN v1.5	35.0	1.4	0.53
GFED4s	56.8	3.3	0.34
GFAS v1.3 <sup>a</sup>	43.2	1.4	0.32
QFED v2.5 <sup>b</sup>	58.5	2.3	0.85
FEER v1.0 <sup>c</sup>	102.5	3.8	0.71
FREM v2 <sup>d</sup>	97	–	–
<i>M</i>	69.0	2.9	0.55
<i>CV</i>	39%	52%	38%
CAMS-ANTHRO v4.1 <sup>e</sup>	28.0	2.3	0.24
CEDS <sub>GBD-MAPS</sub> <sup>f</sup>	25.8	2.5	0.28
DACCIWA <sup>g</sup>	23.7	1.8	0.33
DICE v1.1 <sup>h</sup>	28.5	0.6	0.49
<i>M</i>	26.5	1.8	0.3
<i>CV</i>	8%	47%	33%

Note. *M* = mean, *CV* = coefficient of variation

APA<sup>(a)</sup> Global Fire Assimilation System (Kaiser et al., 2012) version v1.3, downloaded from <ftp://ftp.mpic.de/GFAS/v1p3>. <sup>(b)</sup> Quick Fire Emissions Dataset (Darmenov and da Silva, 2015) version 2.5, downloaded from <http://ftp.as.harvard.edu/gcgrid/data/ExtData/HEMCO/QFED/v2018-07/>. <sup>(c)</sup> Fire Energetics and Emissions Research (Ichoku and Ellison, 2014), FEERv1.0-G1.2 DAILY, downloaded from <https://feer.gsfc.nasa.gov/data/emissions/>. <sup>(d)</sup> Fire Radiative Energy Emissions version 2, values picked from Fig. 10 of (Nguyen and Wooster, 2020). <sup>(e)</sup> Anthropogenic emission totals from the CAMS-ANTHRO v4.1 inventory (Granier et al., 2019), downloaded from <https://eccad.aeris-data.fr/>. <sup>(f)</sup> Updated Community Emissions Data System, described in (McDuffie et al., 2020), and downloaded from <https://zenodo.org/record/3754964#.X5Fe7JNLhE5>. To calculate July-September totals, annual emissions are assumed to be constant over the year. <sup>(g)</sup> Updated Community Emissions Data System, described in (McDuffie et al., 2020), and downloaded from <https://zenodo.org/record/3754964#.X5Fe7JNLhE5>. To calculate July-September totals, annual emissions are assumed to be constant over the year. <sup>(h)</sup> Dynamics-aerosol-chemistry-cloud interactions in West Africa inventory, described in (Knippertz et al., 2015), and downloaded from <https://eccad.aeris-data.fr/>. <sup>(i)</sup> Diffuse and Inefficient Combustion Emissions in Africa v1.1 inventory (Marais and Wiedinmyer, 2016), downloaded from <http://www.acom.ucar.edu/Models/dice-africa/DICE-Africa-2013-v01-4Oct2016.zip>. The inventory refers to 2013 and excludes emissions from the sectors energy production and formal industry. These emissions are substituted with year 2010 estimates from EGDAR v4.3.2 (Crippa et al., 2018). July-September totals from annual inventories are calculated under the assumption that emissions are constant throughout the year. <sup>(j)</sup> NO<sub>x</sub> emissions as NO.

The absolute spread of estimates (max–min range) in the different fire inventories is by a factor of two and larger in the anthropogenic inventories, reflecting that fire emission uncertainty is of foremost relevance when forecasting air quality across Africa.

Among the different fire emission inventories, the two top-down inventories FEER and FIREM yield the highest CO emission totals for the period July to September 2016, followed by FireCCISFD11. Compared to these, emissions estimated by FINN, the inventory with lowest CO emissions, are by a factor of 2.6 to 2.9 lower. The order, however, varies across species. In terms of NO<sub>x</sub>, FireCCISFD11 yields by far the highest emissions, while in terms of BC, FireCCISFD11 emissions ranks at an average level together with FINN. QFED emissions of CO and NO<sub>x</sub> rank at an average level, while QFED BC emissions, due to the extraordinarily high BC emission factors used (Table 4), are highest among all inventories. The rank order can additionally changes over time (Figure 14). CO emissions in FireCCISFD11 in July and August 2016, for example, are lower than in FEER and FIREM, while they are higher than in FIREM in September 2016. This means that the different fire inventories differ in a non-linear manner across species and time. Solely the relation between FireCCISFD11 and GFED4s emissions remains between 49% and 68%, irrespective of the species, and, in the months July and August 2016, the relation within 2% identical with how both products relate in terms of burned area (Table 1). In summary, at a continental scale, monthly FireCCISFD11 and GFED4s emission fluxes are largely proportional.

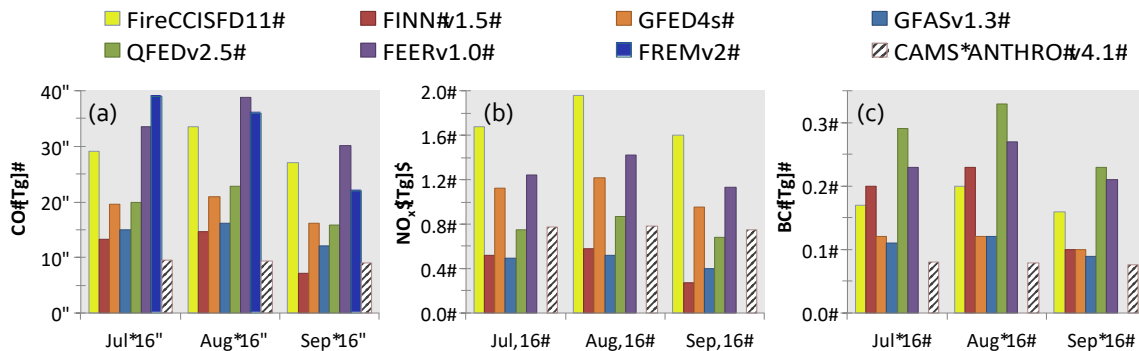


**Figure 14:** Monthly total emissions from fires across Africa (in Tg) during July to September 2016 estimated by different inventories (a) carbon monoxide (CO) and (b) oxides of nitrogen (NO<sub>x</sub>) as NO, and (c) black carbon (BC). Anthropogenic emissions from the CAMS-ANTHRO inventory are shown as well.

At a daily temporal resolution, synchrony between the emission fluxes time series is relatively low (Figure 15). The portion of common variation in the FireCCISFD11 and GFED4s emission fluxes, indicated by the Pearson's  $r^2$ , is 60% (Table 7), reflecting the effect of using different down-sampling approaches to distribute the monthly estimates of these products into daily information (see Section 4.4.2). The temporal correlation with the FINN time series is substantially lower ( $r^2 \leq 34\%$ ), and there is also relatively low correlation with the time series of the FRP-based emission inventories GFAS, QFED and FEER ( $r^2$  between 35% and 57%). Of all inventories, the explained variance is highest ( $r^2=74\%$ ) between the two fully top-down approaches QFED and FEER. The diurnal cycle of fire emissions, in contrast, varies only slightly between GFED4s and FireCCISFD11 on the one side and FINN on the side, because a largely similar parameterisation is applied (Figure 16). It is also noteworthy that the diurnal cycle information provided with GFED4s is constant for a given month, and the FINN diurnal

cycle is constant across time and space, which is a strong simplification of the actual diurnal cycle of emission and adds further uncertainty to the fire emission input estimates used in our WRF-Chem simulations.

This illustrates that the choice of the down-sampling method adds additional uncertainty to the fire emission estimates. This has strong implications for atmospheric chemistry modelling since photochemistry responds non-linearly to temporal variations of emissions (Cohan et al., 2005). It is also relevant for model evaluation against observations at time scale of individual smoke plumes.

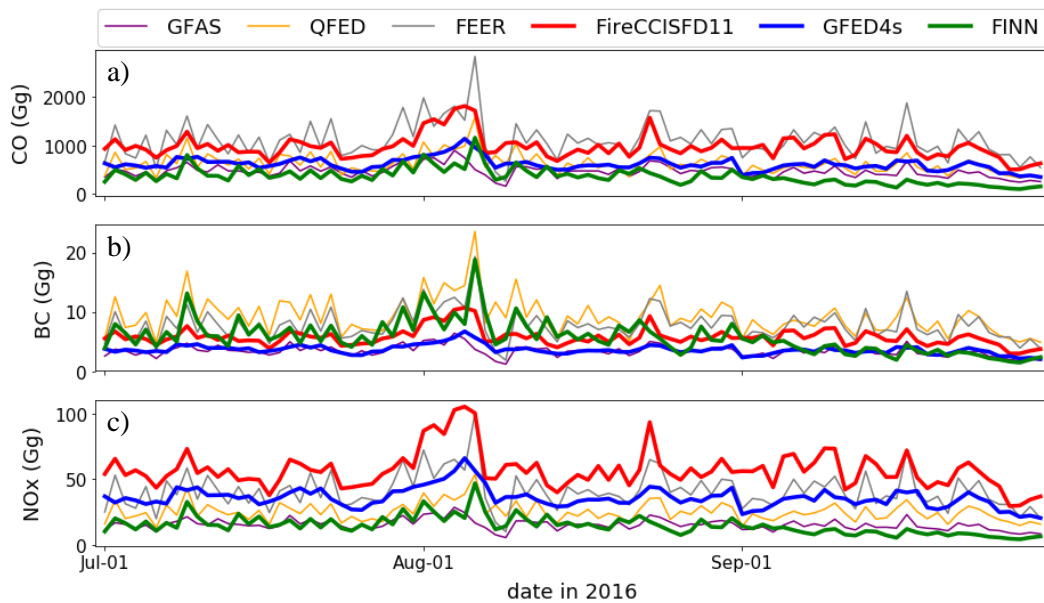


**Figure 15:** Daily total emissions from fires across Africa (in Gg) during July to September 2016 (a) carbon monoxide (CO), (b) black carbon (BC) and (c) oxides of nitrogen ( $\text{NO}_x$  as NO).

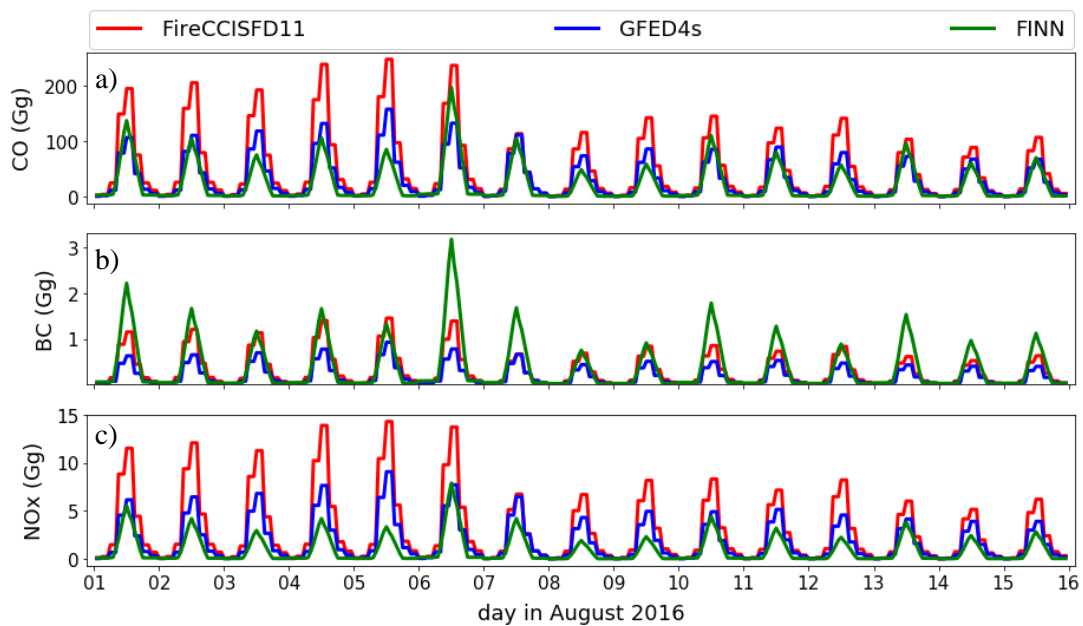


**Figure 16:** Hourly total emissions from fires across Africa (in Gg) in the first half of August 2016 (a) carbon monoxide (CO), (b) black carbon (BC) and (c) oxides of nitrogen ( $\text{NO}_x$  as NO).

**Table 7:** Pearson’s correlation values ( $r^2$ ) between time series of daily total CO emission from fires in Africa (July to September 2016).

Inventory	FireCCISFD11	GFED4s	FINN	GFAS	QFED	FEER
FireCCISFD11	1.0					
GFED4s	.60	1.0				
FINN	.34	.32	1.0			
GFAS	.57	.46	.32	1.0		
QFED	.54	.42	.52	.42	1.0	
FEER	.53	.35	.43	.59	.74	1.0

*Note. n=92*

While there is still substantial uncertainty in the present-day fire emission estimates for Africa, it is much lower than in the fire emission estimates that have been established a decade ago, and that e.g. Williams et al. (2012) used to study the influence of African biomass burning emissions on air quality. Williams et al. (2012)' study focuses on 2006, a year with very comparable fire activity to the year 2016, and comprises the biomass burning emission inventories AMMABB (Lioussé et al., 2010), GFEDv2 (van der Werf et al., 2006) and GFEDv3 (van der Werf et al., 2010). The July to September 2006 AMMABB estimates yield BC emissions of 2.95 Tg and CO emissions of 428 Tg, which are 8–9 times larger than the values estimated by the GFED versions v2 and v3, and also by GFED4s. Granier et al. (2011) state that the much higher burned area estimates of the underlying L3JRC burned area product explain the larger AMMABB emissions.

#### 4.5.1. Sensitivity of emission estimation to fuel type parameterisation

Information on the fuel type is a prerequisite for estimating fire emissions. One option to obtain such information are satellite land cover maps. However, the land cover classes used in these maps do not directly correspond to fuel type classes used in fire emission calculation. Translation is required.

Fuel type is needed to apply emission factors since these are fuel-type dependent. Information on the fuel type burned is also required when fuel consumption is not modelled, but estimated from field measurements of fuel consumption. The fuel type categories classically used in fire emission calculation are savanna (occasionally sometimes divided into grassland and woody savanna), cropland, and tropical, temperate and extratropical forest (Akagi et al., 2011; Andreae, 2019; van Leeuwen et al., 2014).

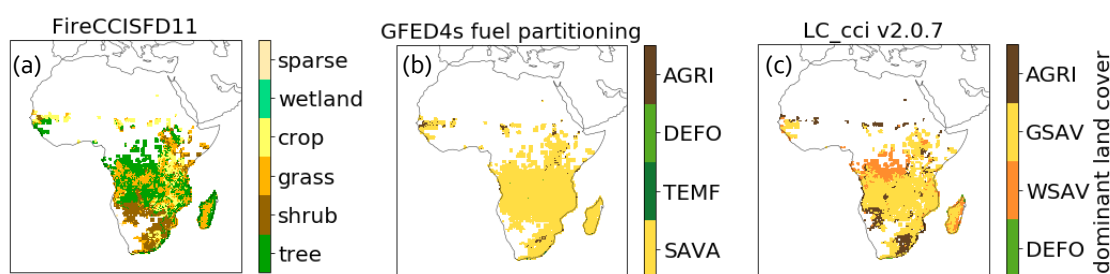
The Fire\_cci burned area products provide explicit information on the type of vegetation that has burned. The FireCCISFD11 product specifies burned area by six land cover classes: trees cover, shrubs cover, grassland, cropland, vegetation aquatic or regularly flooded, and lichen and mosses/sparse vegetation. The land cover information originates from the 20 m resolution CCI Sentinel-2 (S2) prototype Land Cover map for Africa for the year 2016 (<http://2016africalandcover20m.esrin.esa.int/>, accessed on November 2020).

Figure 17a illustrates that across July to September 2016, most fires in FireCCISFD11 occur in areas classified as predominantly tree covered, followed by grassland, shrubland and cropland fires. The figure also illustrates that the general class “tree cover” in the CCI 20-m S2 map encompasses tropical forest but also more sparsely tree covered areas that are commonly categorised as savanna; and hence does not allow a differentiation into savanna and forest fuel types. This is relevant because for fire

emission calculation, tropical forest and savannah areas have to be treated separately. In comparison, with few exceptions, all areas burned in FireCCISFD11 are classified as predominant savanna fuels in GFED4s (Figure 17b) and also in a translated ESA CCI land cover map (Figure 17c).

As a sensitivity test, we calculated fire emissions from the FireCCISFD11 burned area product using the fuel type-dependent estimates of fuel consumption from the van Leeuwen et al. (2014) database and emission factors from the Andreae (2019) compilation (Table 8) in combination with

- (i) the CCI S2 prototype land cover information provided with the FireCCISFD11 product (Figure 17a)
- (ii) the LC\_cci v2.0.7 land cover type of the surfaces burned in FireCCISFD11, obtained by spatial intersection of both products (Figure 17c).



**Figure 17:** Dominant land and fuel cover type in grid cells with FireCCISFD11 fire detections across JAS 2016 using (a) ESA CCI S2 land cover map, (b) the GFED4s fuel partitioning layer, and (c) a translated ESA CCI LC\_cci v2.0.7 land cover map of the year 2015. The translation largely follows ESA (2017), Wang et al. (2019) and Tab. 7 of Bai (2010). Grassland savanna (GSAV) corresponds to the UN-LCCS land cover classes 130 to 150, woody savanna (WSAV) to the classes 60, 110, 120 and 180, and agriculture (AGRI) the classes 10 to 40. The LC\_cci v2.0.7 product consists of annual maps. To classify the land cover type burned across JAS2016, the land cover map of the year 2015 is used since it better reflects the land cover prior the JAS2016 fires than the land cover map of the year 2016.

Table 8 shows that fuel consumption and emission factors are substantially larger for deforestation fires than for e.g. woody savanna fires. As a result, carbon monoxide (CO) emissions per unit mass fuel consumed in deforestation fires is a factor of 37 higher than in woody savanna fires.

Table 9 illustrates that total fire emissions calculated with these two parameterisations are substantially higher than with the GFED4s-like approach we adopted in this study (see sections 4.3). Using the CCI S2 fuel type parameterisation (i) yields, dependent upon the species, 4 to 8 times higher fire emissions. CO and BC emissions in the LC\_cci v2.0.7 fuel type parameterisation (ii) are around 50% higher than in the GFED4s-like approach, while NO<sub>x</sub> emission are 23% lower, primarily because the Andreae (2019) NO<sub>x</sub> emission factor for savanna used in this sensitivity test is 36% lower than in the GFED4s-like approach.

This sensitivity test highlights that fire emission estimation is very sensitive to the choice of the fuel type parameterisation. It also highlights that using alternate approaches to calculate fire emissions from the FireCCISFD11 burned area estimates tend to lead to higher overall fire emissions than in the GFED4s-like approach used in our WRF-Chem study.

**Table 8:** Fuel consumption (FC) and emission factors (EF) estimates from the Andreae (2019) and van Leeuwen et al. (2014) compilations for the four major fuel types in Africa. The first three columns depict how the CCI S2 and the LC\_cci v2.0.7 land cover classes are translated.

Fuel type	CCI S2 (land cover class)	LC_cci v2.0.7 (LCCS code)	FC (km m <sup>-2</sup> )	EF (g kg <sup>-1</sup> )		
				CO	NO <sub>x</sub>	BC
DEFO	Tree cover	50, 70-100, 160-170	126 <sup>a</sup>	104	2.8	0.51
WSAV	Shrub cover	60, 110-120, 180	3.9	69	2.5	0.53
GSAV	Grassland	130-150	3.2			
AGRI	cropland	10-40	6.5 <sup>a</sup>	76	2.4	0.42

<sup>a</sup> Fuel consumption values estimated from similar biomes outside Africa.

**Table 9:** Total emissions from fires across Africa during the period July to September 2016 calculated from FireCCISFD11 burned area using different fuel type parameterisations (see **Table 8**).

	fuel type parameterisation	CO [Tg]	NO <sub>x</sub> [Tg]	BC [Tg]
(i)	CCI S2	855.4	23.3	4.26
(ii)	LC_cci v2.0.7	133.0	4.1	0.79
this study	GFED4s-like	89.9	5.2	0.53

## 5. WRF-Chem model evaluation

We here show first results from the WRF-Chem model simulations using FINN, GFED4s and FireCCISFD11 fire emissions. The simulation with FINN, considered as reference run, show strongly elevated surface concentrations of carbon monoxide (CO) above the major biomass burning regions. CO is an air pollutant created during incomplete combustion of organic material, and, because of its long atmospheric lifetime, is frequently used as tracer for long-range transport of biomass burning plumes (e.g. Williams et al. (2012)). In large regions close to the Equator, daily mean surface CO concentrations exceed 250 ppb (Figure 18a), and CO hourly values occasionally exceed the WHO air quality guideline value of 25 ppm (World Health Organization, 2000). In comparison to this reference run, the simulation with GFED4s and FireCCISFD11 yield largely enhanced surface CO concentrations in the southern hemispheric tropics (Figure 18b and c). Particularly in FireCCISFD11, there is a widespread enhancement by 50% and more.

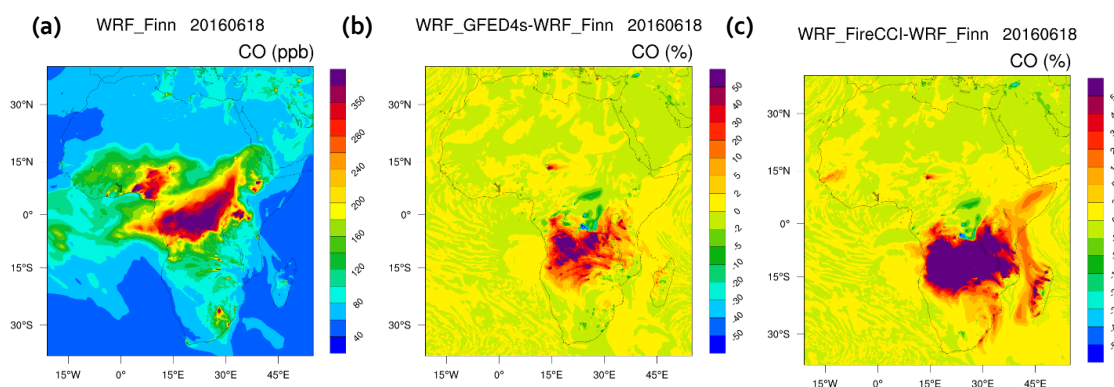


**Figure 18:** (a) Surface carbon monoxide (CO) concentrations modelled with WRF-Chem for June 18, 2016 with FINN fire emissions (reference run). Relative difference with respect to the reference run when using (b) GFED4s and (c) FireCCISFD11 fire emissions.

We also analysed how the GFED4s and FireCCISFD11 simulations for June 18, 2016 differ from the FINN reference run in terms of carbon monoxide vertical profiles along the 13° E cross-section (Figure 19a). Between around 20° to 12° S, CO concentrations in the lower troposphere are strongly enhanced in both simulations (Figure 19 (b, c)). The exception is a region between 14° and 12° S, where, at an altitude band between around 4 and 7 km, CO concentrations in the reference run are, in parts, higher. The reason for this can be twofold: i) FINN surface emission fluxes are locally higher or (ii) the FINN plume rise is locally higher than in the GFED4s or FireCCISFD11 parameterisation.

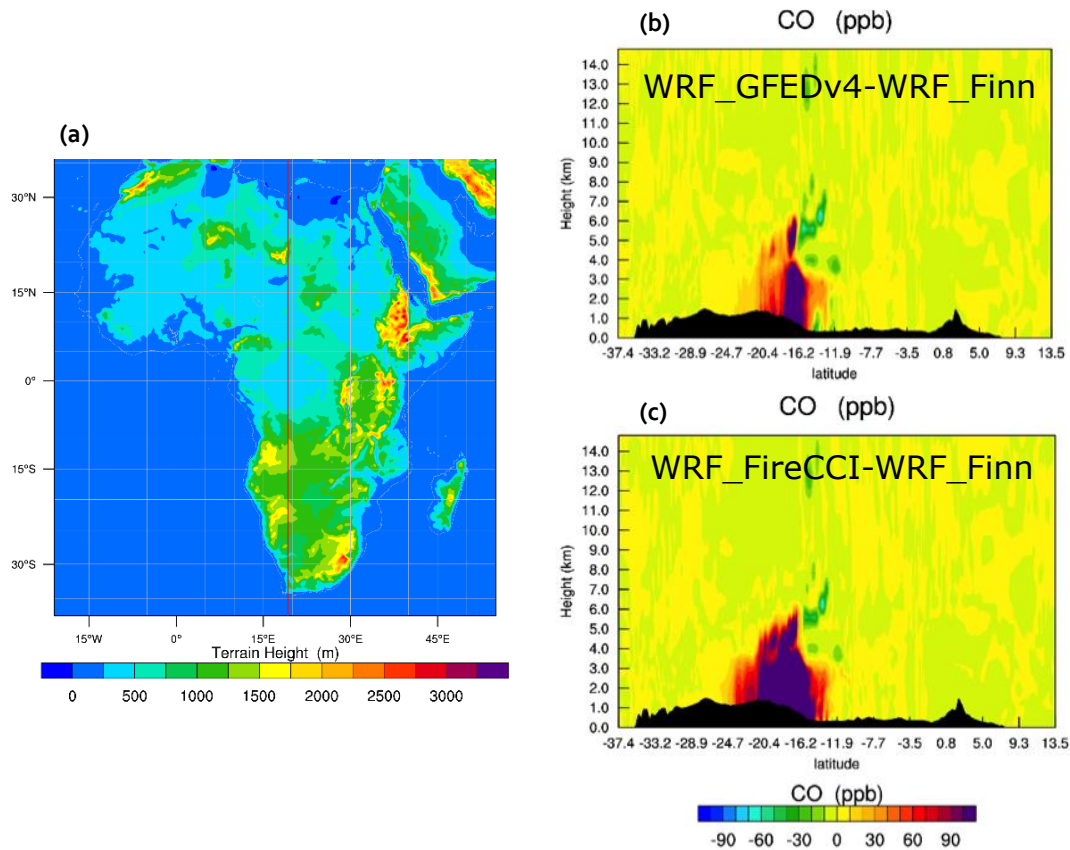
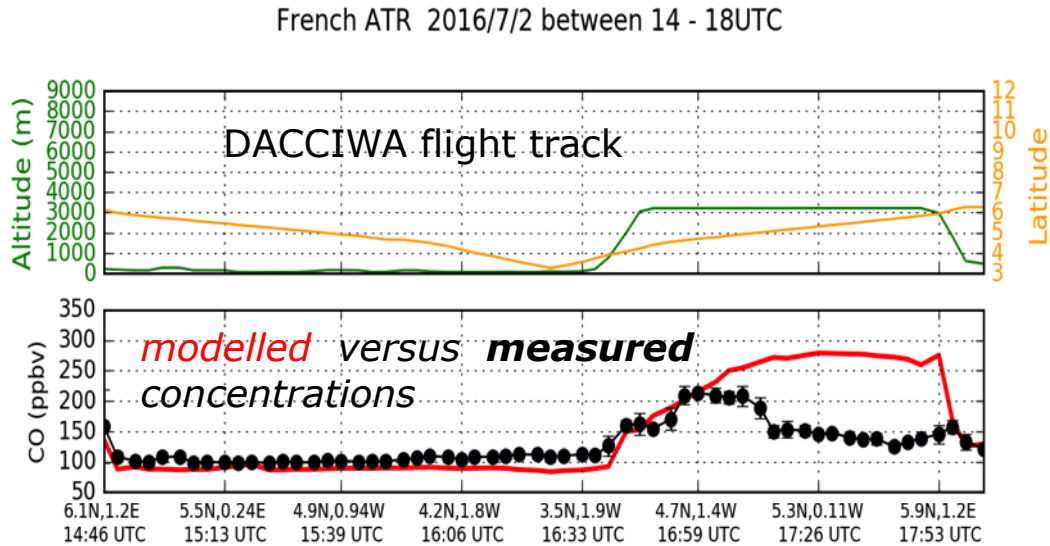


**Figure 19:** (a) Topographic map of the WRF-Chem Africa model domain with line along 19° E indicating the cross-section displayed in (b) and (c). Cross-section showing the vertical distribution of modelled carbon monoxide concentrations for June 18, 2016. Shown is the absolute difference of the simulation with (b) GFED4s and (c) FireCCISFD11 fire emissions, respectively, and the FINN reference run.

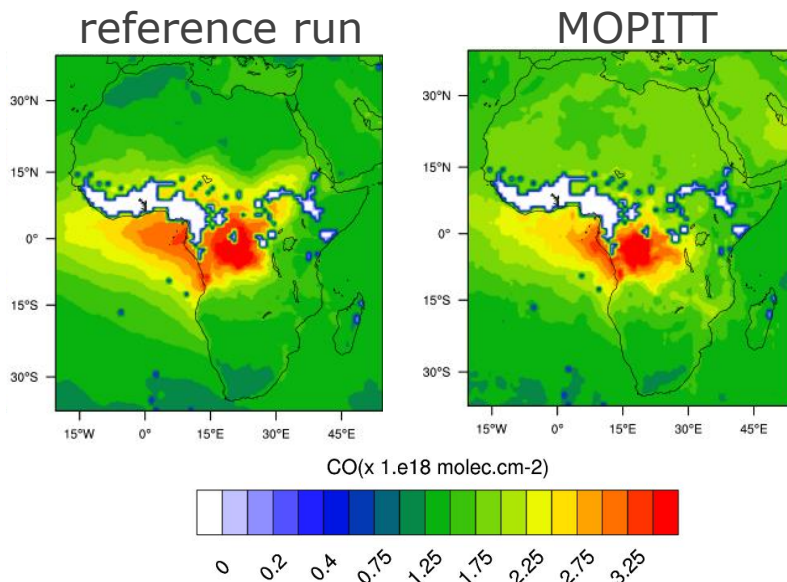
Figure 20 shows the evaluation of the WRF-Chem reference run (with FINN fire emissions) with CO measurements obtained during a DACCIWA flight track on July 2, 2016. DACCIWA (Dynamics-Aerosol-Chemistry-Cloud Interactions in West Africa) is an extensive aircraft measurement campaign conducted over West Africa during June-July 2016 with focus on aerosol-cloud interactions (Knippertz et al., 2017). Backward trajectories calculated with WRF (Flamant et al., 2018) suggests that some of the air masses sampled during DACCIWA were influenced by long-range transport of biomass burning emissions from central Africa.

Figure 20 shows that the WRF-Chem reference run captures well the biomass burning plume (indicated by elevated CO levels) that was encountered during the flight track along the coast of Ghana at around 4:40 pm UTC. The model, however, then overestimates the concentrations within the plume by around 100 ppb.

An overestimation in modelled CO concentrations is also observed over July 2016 in the region around the Gulf of Guinea when comparing the WRF-Chem reference simulation with CO columns from the satellite-derived MOPITT (Measurement of Pollution in the Troposphere) dataset (Figure 21). The comparison shows, that despite this, the general spatial pattern of biomass burning-related enhanced CO levels is well captured by the model.



**Figure 20:** Comparison of CO concentrations modelled by WRF-Chem in the reference run (FINN fire emissions) with those measured by the DACCIWA aircraft measurement campaign on July 2, 2016 over coastal Ghana. (a) displays the flight track including flight height and latitude information, and (b) the concentrations along the flight track.



**Figure 21:** Comparison of CO atmospheric columns modelled by WRF-Chem in the reference run (FINN fire emissions) with MOPITT observations for July 2016.

 <b>fire</b> cci	<b>Fire_cci</b> <b>Climate Assessment Report</b>		Ref.	Fire_cci_D5.1_CAR_v2.1	
			Issue	2.1	Date
				Page	37

The preliminary evaluation of results from the WRF-Chem reference run with observations provides no indication of FINN underestimating fire emissions. On the contrary, we found indications for modelled CO concentrations overestimating the observed CO concentrations in the biomass burning plumes. We presume that the overestimation will be even more pronounced in the simulations using GFED4s and FireCCISFD11 fire emissions, pointing to a potential overestimation in these fire emission inventories.

As a next step, we will more thoroughly evaluate modelled atmospheric concentrations using the different fire emission inventories against satellite, aircraft, and surface observations. In addition, we will evaluate the results against Copernicus Atmosphere Monitoring Service (CAMS) chemical reanalysis.

## 6. Conclusions

We assessed the suitability of the Fire\_cci FireCCISFD11 burned area product for atmospheric chemistry modelling with the regional WRF-CHEM model. To our knowledge, this is the first application of a Fire\_cci product for this kind of application.

There are several reasons why atmospheric chemistry modellers do not take advantage from the fire information provided with the Fire\_cci products since two key requirements are not met:

### *(1) Availability of ready-to-use fire emissions:*

Atmospheric chemistry modellers use fire information to prescribe the surface emission fluxes to the model. They generally prefer using ready-to-use fire emission inventories instead of having to create them on their own from scratch.

### *(2) Availability of a fire emission pre-processor:*

For use as input in atmospheric chemistry models, the fire emission data have to be converted into the specific input data format of the model. This conversion includes e.g., mass-conserving remapping of the emissions into the curvilinear grid of the model, the mapping of fire emissions to the speciation used in the model, the addition of a diurnal cycle and of specific layers (e.g. fire size), and formatting file structure and attributes. Because building such a pre-processor is time-consuming and error-prone, atmospheric chemistry modellers tend to use fire emission input for which a pre-processor is already available.

If atmospheric chemistry modellers shall become an important user group of Fire\_cci products, then it would be necessary to provide Fire\_cci emission products together with pre-processing tools.

In this work, we computed fire emissions from burned area information contained in the Fire\_cci FireCCISFD11 grid product and pre-processed them so that they can be used as fire emission input in the WRF-Chem model. While doing so, we encountered several difficulties, which we discuss in the following paragraphs:

- The 0.25° spatial resolution of the Fire\_cci grid products is too coarse for use in regional atmospheric chemistry model simulations. The latter are typically set up with a curvilinear grid that has a spatial resolution close to or higher than that of the grid products. Mass-conserving spatial interpolation of the 0.25° gridded data to the curvilinear grid is difficult and entails unavoidable spatial gradient errors. Optimal results are achieved when spatially interpolating burned area information from the

 <b>fire</b> cci	<b>Fire_cci</b> <b>Climate Assessment Report</b>		Ref.	Fire_cci_D5.1_CAR_v2.1	
			Issue	2.1	Date
				Page	38

Fire\_cci pixel products, however, this requires knowledge on how to process tiled Geotiff-files, which atmospheric modellers typically do not have, it involves substantial pre-processing and is computationally demanding. There is no guidance or sample code on how to best remap the Fire\_cci pixel products to a custom grid product; its provision would be very beneficial to atmospheric chemistry users, though. An alternative would be to deliver Fire\_cci grid products with higher spatial resolution allowing users to remap with conventional remapping algorithms (e.g. bilinear interpolation) with low interpolation errors. For spatial resolutions typically used in regional atmospheric models, a grid resolution of  $0.05^\circ$  would be optimal.

- The monthly temporal resolution of the Fire\_cci grid products is insufficient for use in atmospheric chemistry models, which require hourly time resolution of fire emission input data. To enhance the update of Fire\_cci products by atmospheric chemistry modellers, it would be advisable to provide temporal scalars as ancillary product layer which provide information on how to convert monthly into hourly burned area, analogous to what is provided in GFED4s.
- WRF-Chem fire emission input requires information on the fire size. For this purpose, we explored the number of burn patches data layer provided with the Fire\_cci grid products since the quotient of the area burned and the burn patch number should theoretically provide an indicator of the mean fire size. Our analysis, however, showed that the number of burn patches provided with the Fire\_cci products is unrealistically high, pointing to an error in the computation algorithm of this information. We therefore recommend to either remove this layer or to recompute this layer with a corrected algorithm.
- Calculating fire emissions requires information on the fuel type burned. While the Fire\_cci grid products provide information of the area burned by land cover type, the 20 m resolution CCI S2 land cover map underlying the FireCCISFD11 product was found unsuitable for discriminating different fuel types. Most importantly, it does not allow discriminating between tropical forest and savanna fires, which is crucial for emission factor parameterisation. We therefore recommend using e.g. the UN-LCCS land cover type information from the ESA LC\_cci v2.0.7 land cover product, which, despite its lower spatial resolution (300 m versus 20 m) allows a clear delineation between different fuel types.

We performed WRF-Chem simulations over Africa with three fire emission inventories: FINN, GFED4s, and FireCCISFD11. A preliminary evaluation of modelled atmospheric concentrations of individual species emitted by the fires against observations point to a substantial overestimation of fire emissions in GFED4s and, in particular, FireCCISFD11. The most likely reasons for this overestimation are either that the underlying burned area rates are too large and/or the underlying GFED4s fuel consumption parameterisation is high-biased. We also tested two alternate approaches to calculate fire emissions from FireCCISFD11 burned area, and in both, fire emissions tend to be even much larger. Some of the overestimation could be related to the model not adequately predicting the actual emission height of the smoke plumes; however, this cannot explain, e.g. the over-prediction of observed vertically-integrated column concentrations of carbon monoxide (CO).

So far, studies evaluating GFED4s fuel consumption rates are contradictory: Wees and van der Werf (2019) studied the effect of spatial resolution on biomass burning emissions modelled by the GFED framework for the African continent. They did specific adaptations to the GFED setup and performed model optimization using satellite-based reference data and field measurements of fuel load and fuel consumption. Their results

	<b>Fire_cci</b> <b>Climate Assessment Report</b>		Ref.	Fire_cci_D5.1_CAR_v2.1	
			Issue	2.1	Date
					Page

indicate that fuel consumption in GFED4s is overestimated by 24%. In contrast to this, Nguyen and Wooster (2020) deduced fuel consumption by combining satellite observations of fire radiative power (FRP) and aerosol optical depths (AOD) and their results point to GFED4s underestimating fuel consumption.

The detailed analysis and interpretation of the WRF-Chem model results will be included in a forthcoming publication.

## 7. References

Akagi, S. K., Yokelson, R. J., Wiedinmyer, C., Alvarado, M. J., Reid, J. S., Karl, T., Crouse, J. D. and Wennberg, P. O.: Emission factors for open and domestic biomass burning for use in atmospheric models, *Atmospheric Chem. Phys.*, 11(9), 4039–4072, doi:10.5194/acp-11-4039-2011, 2011.

Andela, N., Morton, D. C., Giglio, L., Chen, Y., van der Werf, G. R., Kasibhatla, P. S., DeFries, R. S., Collatz, G. J., Hantson, S., Kloster, S., Bachelet, D., Forrest, M., Lasslop, G., Li, F., Mangeon, S., Melton, J. R., Yue, C. and Randerson, J. T.: A human-driven decline in global burned area, *Science*, 356(6345), 1356–1362, doi:10.1126/science.aal4108, 2017.

Andela, N., Morton, D. C., Giglio, L., Paugam, R., Chen, Y., Hantson, S., van der Werf, G. R. and Randerson, J. T.: The Global Fire Atlas of individual fire size, duration, speed and direction, *Earth Syst. Sci. Data*, 11(2), 529–552, doi:10.5194/essd-11-529-2019, 2019.

Andreae, M. O.: Emission of trace gases and aerosols from biomass burning – an updated assessment, *Atmospheric Chem. Phys.*, 19(13), 8523–8546, doi:10.5194/acp-19-8523-2019, 2019.

Andreae, M. O. and Merlet, P.: Emission of trace gases and aerosols from biomass burning, *Glob. Biogeochem. Cycles*, 15(4), 955–966, doi:10.1029/2000GB001382, 2001.

Aurela, M., Beukes, J. P., van Zyl, P., Vakkari, V., Teinilä, K., Saarikoski, S. and Laakso, L.: The composition of ambient and fresh biomass burning aerosols at a savannah site, South Africa, *South Afr. J. Sci.*, Volume 112(Number 5/6), doi:10.17159/sajs.2016/20150223, 2016.

Bai, L.: Comparison and Validation of Five Land Cover Products over the African Continent, [online] Available from: <http://lup.lub.lu.se/luur/download?func=downloadFile&recordId=1969905&fileId=1969934> (Accessed 18 February 2019), 2010.

Barten, J. G. M., Ganzeveld, L. N., Visser, A. J., Jiménez, R. and Krol, M. C.: Evaluation of nitrogen oxides (NO<sub>x</sub>) sources and sinks and ozone production in Colombia and surrounding areas, *Atmospheric Chem. Phys.*, 20(15), 9441–9458, doi:10.5194/acp-20-9441-2020, 2020.

Bauer, S. E., Im, U., Mezuman, K. and Gao, C. Y.: Desert Dust, Industrialization, and Agricultural Fires: Health Impacts of Outdoor Air Pollution in Africa, *J. Geophys. Res. Atmospheres*, 124(7), 4104–4120, doi:10.1029/2018JD029336, 2019.

	<b>Fire_cci</b> <b>Climate Assessment Report</b>		Ref.	Fire_cci_D5.1_CAR_v2.1	
			Issue	2.1	Date
				Page	40

Bennet, C. and Engardt, M.: A regional model for surface ozone in Southeast Asia, *Tellus B Chem. Phys. Meteorol.*, 60(5), 718–728, doi:10.1111/j.1600-0889.2008.00378.x, 2008.

Bi, X., Dai, Q., Wu, J., Zhang, Q., Zhang, W., Luo, R., Cheng, Y., Zhang, J., Wang, L., Yu, Z., Zhang, Y., Tian, Y. and Feng, Y.: Characteristics of the main primary source profiles of particulate matter across China from 1987 to 2017, *Atmospheric Chem. Phys.*, 19(5), 3223–3243, doi:10.5194/acp-19-3223-2019, 2019.

Bouarar, I., Brasseur, G., Petersen, K., Granier, C., Fan, Q., Wang, X., Wang, L., Ji, D., Liu, Z., Xie, Y., Gao, W. and Elguindi, N.: Influence of anthropogenic emission inventories on simulations of air quality in China during winter and summer 2010, *Atmos. Environ.*, 198, 236–256, doi:10.1016/j.atmosenv.2018.10.043, 2019.

Castellanos, P., Boersma, K. F. and van der Werf, G. R.: Satellite observations indicate substantial spatiotemporal variability in biomass burning NO<sub>x</sub> emission factors for South America, *Atmospheric Chem. Phys.*, 14(8), 3929–3943, doi:10.5194/acp-14-3929-2014, 2014.

Cohan, D. S., Hakami, A., Hu, Y. and Russell, A. G.: Nonlinear Response of Ozone to Emissions: Source Apportionment and Sensitivity Analysis, *Environ. Sci. Technol.*, 39(17), 6739–6748, doi:10.1021/es048664m, 2005.

Crippa, M., Guizzardi, D., Muntean, M., Schaaf, E., Dentener, F., Aardenne, J. A. van, Monni, S., Doering, U., Olivier, J. G. J., Pagliari, V. and Janssens-Maenhout, G.: Gridded emissions of air pollutants for the period 1970–2012 within EDGAR v4.3.2, *Earth Syst. Sci. Data*, 10(4), 1987–2013, doi:https://doi.org/10.5194/essd-10-1987-2018, 2018.

Darmenov, A. and da Silva, A.: The Quick Fire Emissions Dataset (QFED): Documentation of Versions 2.1, 2.2 and 2.4. Volume 38;, NASA Global Modeling and Assimilation Office, Greenbelt, US. [online] Available from: <https://gmao.gsfc.nasa.gov/pubs/docs/Darmenov796.pdf> (Accessed 20 October 2020), 2015.

Elguindi, N., Granier, C., Stavrou, T., Darras, S., Bauwens, M., Cao, H., Chen, C., Gon, H. A. C. D. van der, Dubovik, O., Fu, T. M., Henze, D. K., Jiang, Z., Keita, S., Kuenen, J. J. P., Kurokawa, J., Lioussé, C., Miyazaki, K., Müller, J.-F., Qu, Z., Solmon, F. and Zheng, B.: Intercomparison of Magnitudes and Trends in Anthropogenic Surface Emissions From Bottom-Up Inventories, Top-Down Estimates, and Emission Scenarios, *Earths Future*, 8(8), e2020EF001520, doi:10.1029/2020EF001520, 2020.

Emmons, L. K., Schwantes, R. H., Orlando, J. J., Tyndall, G., Kinnison, D., Lamarque, J., Marsh, D., Mills, M. J., Tilmes, S., Bardeen, C., Buchholz, R. R., Conley, A., Gettelman, A., Garcia, R., Simpson, I., Blake, D. R., Meinardi, S. and Pétron, G.: The Chemistry Mechanism in the Community Earth System Model Version 2 (CESM2), *J. Adv. Model. Earth Syst.*, 12(4), doi:10.1029/2019MS001882, 2020.

ESA: Land Cover CCI Product User Guide Version 2.0. [online] Available from: [http://maps.elie.ucl.ac.be/CCI/viewer/download/ESACCI-LC-Ph2-PUGv2\\_2.0.pdf](http://maps.elie.ucl.ac.be/CCI/viewer/download/ESACCI-LC-Ph2-PUGv2_2.0.pdf) (Accessed 7 February 2019), 2017.

	<b>Fire_cci</b> <b>Climate Assessment Report</b>		Ref.	Fire_cci_D5.1_CAR_v2.1		
			Issue	2.1	Date	16/11/2020
			Page		41	

Ferek, R. J., Reid, J. S., Hobbs, P. V., Blake, D. R. and Lioussé, C.: Emission factors of hydrocarbons, halocarbons, trace gases and particles from biomass burning in Brazil, *J. Geophys. Res. Atmospheres*, 103(D24), 32107–32118, doi:10.1029/98JD00692, 1998.

Flamant, C., Deroubaix, A., Chazette, P., Brito, J., Gaetani, M., Knippertz, P., Fink, A. H., de Coetlogon, G., Menut, L., Colomb, A., Denjean, C., Meynadier, R., Rosenberg, P., Dupuy, R., Dominutti, P., Duplissy, J., Bourriane, T., Schwarzenboeck, A., Ramonet, M. and Totems, J.: Aerosol distribution in the northern Gulf of Guinea: local anthropogenic sources, long-range transport, and the role of coastal shallow circulations, *Atmospheric Chem. Phys.*, 18(16), 12363–12389, doi:10.5194/acp-18-12363-2018, 2018.

Freitas, S. R., Longo, K. M., Alonso, M. F., Pirre, M., Marecal, V., Grell, G., Stockler, R., Mello, R. F. and Sánchez Gácita, M.: PREP-CHEM-SRC – 1.0: a preprocessor of trace gas and aerosol emission fields for regional and global atmospheric chemistry models, *Geosci. Model Dev.*, 4(2), 419–433, doi:10.5194/gmd-4-419-2011, 2011.

Friedl, M. A., Sulla-Menashe, D., Tan, B., Schneider, A., Ramankutty, N., Sibley, A. and Huang, X.: MODIS Collection 5 global land cover: Algorithm refinements and characterization of new datasets, *Remote Sens. Environ.*, 114(1), 168–182, doi:10.1016/j.rse.2009.08.016, 2010.

Fu, Y., Li, R., Wang, X., Bergeron, Y., Valeria, O., Chavardès, R. D., Wang, Y. and Hu, J.: Fire Detection and Fire Radiative Power in Forests and Low-Biomass Lands in Northeast Asia: MODIS versus VIIRS Fire Products, *Remote Sens.*, 12(18), 2870, doi:10.3390/rs12182870, 2020.

Giglio, L., Randerson, J. T. and van der Werf, G. R.: Analysis of daily, monthly, and annual burned area using the fourth-generation global fire emissions database (GFED4): ANALYSIS OF BURNED AREA, *J. Geophys. Res. Biogeosciences*, 118(1), 317–328, doi:10.1002/jgrg.20042, 2013.

Giglio, L., Boschetti, L., Roy, D., Humber, M. and Justice, C.: The Collection 6 MODIS burned area mapping algorithm and product, *Remote Sens. Environ.*, 217, 72–85, doi:10.1016/j.rse.2018.08.005, 2018.

Granier, C., Bessagnet, B., Bond, T., D'Angiola, A., Denier van der Gon, H., Frost, G. J., Heil, A., Kaiser, J. W., Kinne, S., Klimont, Z., Kloster, S., Lamarque, J.-F., Lioussé, C., Masui, T., Meleux, F., Mieville, A., Ohara, T., Raut, J.-C., Riahi, K., Schultz, M. G., Smith, S. J., Thompson, A., van Aardenne, J., van der Werf, G. R. and van Vuuren, D. P.: Evolution of anthropogenic and biomass burning emissions of air pollutants at global and regional scales during the 1980–2010 period, *Clim. Change*, 109(1–2), 163–190, doi:10.1007/s10584-011-0154-1, 2011.

Granier, C., Darras, S., Denier van der Gon, H., Doubalova, J., Elguindi, N., Galle, B., Gauss, M., Guevara, M., Jalkanen, J.-P., Kuenen, J., Lioussé, C., Quack, B., Simpson, D. and Sindelarova, K.: The Copernicus Atmosphere Monitoring Service global and regional emissions (April 2019 version), , doi:10.24380/D0BN-KX16, 2019.

	<b>fire</b> cci	<b>Fire_cci</b>		Ref.	Fire_cci_D5.1_CAR_v2.1		
		<b>Climate Assessment Report</b>		Issue	2.1	Date	16/11/2020
						Page	42

Grell, G., Freitas, S. R., Stuefer, M. and Fast, J.: Inclusion of biomass burning in WRF-Chem: impact of wildfires on weather forecasts, *Atmospheric Chem. Phys.*, 11(11), 5289–5303, doi:10.5194/acp-11-5289-2011, 2011.

Grell, G. A., Peckham, S. E., Schmitz, R., McKeen, S. A., Frost, G., Skamarock, W. C. and Eder, B.: Fully coupled “online” chemistry within the WRF model, *Atmos. Environ.*, 39(37), 6957–6975, doi:10.1016/j.atmosenv.2005.04.027, 2005.

Guevara, M., Tena, C., Porquet, M., Jorba, O. and Pérez García-Pando, C.: HERMESv3, a stand-alone multi-scale atmospheric emission modelling framework – Part 1: global and regional module, *Geosci. Model Dev.*, 12(5), 1885–1907, doi:10.5194/gmd-12-1885-2019, 2019.

Heil, A.: ESA CCI ECV Fire Disturbance: D1.1 User requirements document, version 6.0. [online] Available from: <https://www.esa-fire-cci.org/documents> (Accessed 18 February 2020), 2019.

Hodnebrog, Ø., Solberg, S., Stordal, F., Svendby, T. M., Simpson, D., Gauss, M., Hilboll, A., Pfister, G. G., Turquety, S., Richter, A., Burrows, J. P. and Denier van der Gon, H. A. C.: Impact of forest fires, biogenic emissions and high temperatures on the elevated Eastern Mediterranean ozone levels during the hot summer of 2007, *Atmospheric Chem. Phys.*, 12(18), 8727–8750, doi:10.5194/acp-12-8727-2012, 2012.

Holanda, B. A., Pöhlker, M. L., Walter, D., Saturno, J., Sörgel, M., Ditas, J., Ditas, F., Schulz, C., Franco, M. A., Wang, Q., Donth, T., Artaxo, P., Barbosa, H. M. J., Borrmann, S., Braga, R., Brito, J., Cheng, Y., Dollner, M., Kaiser, J. W., Klimach, T., Knote, C., Krüger, O. O., Fütterer, D., Lavrič, J. V., Ma, N., Machado, L. A. T., Ming, J., Morais, F. G., Paulsen, H., Sauer, D., Schlager, H., Schneider, J., Su, H., Weinzierl, B., Walser, A., Wendisch, M., Ziereis, H., Zöger, M., Pöschl, U., Andreae, M. O. and Pöhlker, C.: Influx of African biomass burning aerosol during the Amazonian dry season through layered transatlantic transport of black carbon-rich smoke, *Atmospheric Chem. Phys.*, 20(8), 4757–4785, doi:10.5194/acp-20-4757-2020, 2020.

Ichoku, C. and Ellison, L.: Global top-down smoke-aerosol emissions estimation using satellite fire radiative power measurements, *Atmospheric Chem. Phys.*, 14(13), 6643–6667, doi:10.5194/acp-14-6643-2014, 2014.

Janssens-Maenhout, G., Crippa, M., Guizzardi, D., Muntean, M., Schaaf, E., Dentener, F., Bergamaschi, P., Pagliari, V., Olivier, J. G. J., Peters, J. A. H. W., van Aardenne, J. A., Monni, S., Doering, U., Petrescu, A. M. R., Solazzo, E. and Oreggioni, G. D.: EDGAR v4.3.2 Global Atlas of the three major greenhouse gas emissions for the period 1970–2012, *Earth Syst. Sci. Data*, 11(3), 959–1002, doi:10.5194/essd-11-959-2019, 2019.

Jones, P. W.: First- and Second-Order Conservative Remapping Schemes for Grids in Spherical Coordinates, *Mon. Weather Rev.*, 127(9), 2204–2210, doi:10.1175/1520-0493(1999)127<2204:FASOCR>2.0.CO;2, 1999.

Kahiu, M. N. and Hanan, N. P.: Fire in sub-Saharan Africa: The fuel, cure and connectivity hypothesis, *Glob. Ecol. Biogeogr.*, 27(8), 946–957, doi:10.1111/geb.12753, 2018.

 <b>fire</b> cci	<b>Fire_cci</b>		Ref.	Fire_cci_D5.1_CAR_v2.1		
	<b>Climate Assessment Report</b>		Issue	2.1	Date	16/11/2020
					Page	43

Kaiser, J. W., Heil, A., Andreae, M. O., Benedetti, A., Chubarova, N., Jones, L., Morcrette, J.-J., Razinger, M., Schultz, M. G., Suttie, M. and van der Werf, G. R.: Biomass burning emissions estimated with a global fire assimilation system based on observed fire radiative power, *Biogeosciences*, 9(1), 527–554, doi:10.5194/bg-9-527-2012, 2012.

Kim, K.-H., Shim, P.-S. and Shin, S.: An Alternative Bilinear Interpolation Method Between Spherical Grids, *Atmosphere*, 10(3), 123, doi:10.3390/atmos10030123, 2019.

Knippertz, P., Coe, H., Chiu, J. C., Evans, M. J., Fink, A. H., Kalthoff, N., Liousse, C., Mari, C., Allan, R. P., Brooks, B., Danour, S., Flamant, C., Jegede, O. O., Lohou, F. and Marsham, J. H.: The DACCIWA Project: Dynamics–Aerosol–Chemistry–Cloud Interactions in West Africa, *Bull. Am. Meteorol. Soc.*, 96(9), 1451–1460, doi:10.1175/BAMS-D-14-00108.1, 2015.

Knippertz, P., Fink, A. H., Deroubaix, A., Morris, E., Tocquer, F., Evans, M. J., Flamant, C., Gaetani, M., Lavaysse, C., Mari, C., Marsham, J. H., Meynadier, R., Affo-Dogo, A., Bahaga, T., Brosse, F., Deetz, K., Guebsi, R., Latifou, I., Maranan, M., Rosenberg, P. D. and Schlueter, A.: A meteorological and chemical overview of the DACCIWA field campaign in West Africa in June–July 2016, *Atmospheric Chem. Phys.*, 17(17), 10893–10918, doi:10.5194/acp-17-10893-2017, 2017.

Koss, A. R., Sekimoto, K., Gilman, J. B., Selimovic, V., Coggon, M. M., Zarzana, K. J., Yuan, B., Lerner, B. M., Brown, S. S., Jimenez, J. L., Krechmer, J., Roberts, J. M., Warneke, C., Yokelson, R. J. and de Gouw, J.: Non-methane organic gas emissions from biomass burning: identification, quantification, and emission factors from PTR-ToF during the FIREX 2016 laboratory experiment, *Atmospheric Chem. Phys.*, 18(5), 3299–3319, doi:10.5194/acp-18-3299-2018, 2018.

Kuik, F., Lauer, A., Beukes, J. P., Van Zyl, P. G., Josipovic, M., Vakkari, V., Laakso, L. and Feig, G. T.: The anthropogenic contribution to atmospheric black carbon concentrations in southern Africa: a WRF-Chem modeling study, *Atmospheric Chem. Phys.*, 15(15), 8809–8830, doi:10.5194/acp-15-8809-2015, 2015.

Laurent, P., Mouillot, F., Yue, C., Ciais, P., Moreno, M. V. and Nogueira, J. M. P.: FRY, a global database of fire patch functional traits derived from space-borne burned area products, *Sci. Data*, 5(1), 180132, doi:10.1038/sdata.2018.132, 2018.

van Leeuwen, T. T., van der Werf, G. R., Hoffmann, A. A., Detmers, R. G., Rücker, G., French, N. H. F., Archibald, S., Carvalho Jr., J. A., Cook, G. D., de Groot, W. J., Hély, C., Kasischke, E. S., Kloster, S., McCarty, J. L., Pettinari, M. L., Savadogo, P., Alvarado, E. C., Boschetti, L., Manuri, S., Meyer, C. P., Siegert, F., Trollope, L. A. and Trollope, W. S. W.: Biomass burning fuel consumption rates: a field measurement database, *Biogeosciences*, 11(24), 7305–7329, doi:https://doi.org/10.5194/bg-11-7305-2014, 2014.

Li, F., Zhang, X., Roy, D. P. and Kondragunta, S.: Estimation of biomass-burning emissions by fusing the fire radiative power retrievals from polar-orbiting and geostationary satellites across the conterminous United States, *Atmos. Environ.*, 211, 274–287, doi:10.1016/j.atmosenv.2019.05.017, 2019.

	<b>Fire_cci</b> <b>Climate Assessment Report</b>	Ref.	Fire_cci_D5.1_CAR_v2.1		
		Issue	2.1	Date	16/11/2020
				Page	44

Li, F., Zhang, X. and Kondragunta, S.: Biomass Burning in Africa: An Investigation of Fire Radiative Power Missed by MODIS Using the 375 m VIIRS Active Fire Product, *Remote Sens.*, 12(10), 1561, doi:10.3390/rs12101561, 2020.

Li, X., Wang, S., Duan, L., Hao, J., Li, C., Chen, Y. and Yang, L.: Particulate and Trace Gas Emissions from Open Burning of Wheat Straw and Corn Stover in China, *Environ. Sci. Technol.*, 41(17), 6052–6058, doi:10.1021/es0705137, 2007.

Liousse, C., Guillaume, B., Grégoire, J. M., Mallet, M., Galy, C., Pont, V., Akpo, A., Bedou, M., Castéra, P., Dungall, L., Gardrat, E., Granier, C., Konaré, A., Malavelle, F., Mariscal, A., Mieville, A., Rosset, R., Serça, D., Solmon, F., Tummon, F., Assamoi, E., Yoboué, V. and Van Velthoven, P.: Updated African biomass burning emission inventories in the framework of the AMMA-IDAF program, with an evaluation of combustion aerosols, *Atmospheric Chem. Phys.*, 10(19), 9631–9646, doi:10.5194/acp-10-9631-2010, 2010.

Lizundia-Loiola, J., Otón, G., Ramo, R. and Chuvieco, E.: A spatio-temporal active-fire clustering approach for global burned area mapping at 250 m from MODIS data, *Remote Sens. Environ.*, 236, 111493, doi:10.1016/j.rse.2019.111493, 2020.

Lu, X., Zhang, X., Li, F. and Cochrane, M. A.: Investigating Smoke Aerosol Emission Coefficients Using MODIS Active Fire and Aerosol Products: A Case Study in the CONUS and Indonesia, *J. Geophys. Res. Biogeosciences*, 124(6), 1413–1429, doi:10.1029/2018JG004974, 2019.

Marais, E. A. and Wiedinmyer, C.: Air Quality Impact of Diffuse and Inefficient Combustion Emissions in Africa (DICE-Africa), *Environ. Sci. Technol.*, 50(19), 10739–10745, doi:10.1021/acs.est.6b02602, 2016.

McDuffie, E. E., Smith, S. J., O'Rourke, P., Tibrewal, K., Venkataraman, C., Marais, E. A., Zheng, B., Crippa, M., Brauer, M. and Martin, R. V.: A global anthropogenic emission inventory of atmospheric pollutants from sector- and fuel-specific sources (1970–2017): An application of the Community Emissions Data System (CEDS), preprint, *Antroposphere - Energy and Emissions.*, 2020.

Mebust, A. K., Russell, A. R., Hudman, R. C., Valin, L. C. and Cohen, R. C.: Characterization of wildfire NO<sub>x</sub> emissions using MODIS fire radiative power and OMI tropospheric NO<sub>2</sub> columns, *Atmospheric Chem. Phys.*, 11(12), 5839–5851, doi:10.5194/acp-11-5839-2011, 2011.

Mu, M., Randerson, J. T., van der Werf, G. R., Giglio, L., Kasibhatla, P., Morton, D., Collatz, G. J., DeFries, R. S., Hyer, E. J., Prins, E. M., Griffith, D. W. T., Wunch, D., Toon, G. C., Sherlock, V. and Wennberg, P. O.: Daily and 3-hourly variability in global fire emissions and consequences for atmospheric model predictions of carbon monoxide: DAILY AND HOURLY GLOBAL FIRE EMISSIONS, *J. Geophys. Res. Atmospheres*, 116(D24), n/a-n/a, doi:10.1029/2011JD016245, 2011.

Nguyen, H. M. and Wooster, M. J.: Advances in the estimation of high Spatio-temporal resolution pan-African top-down biomass burning emissions made using geostationary fire radiative power (FRP) and MAIAC aerosol optical depth (AOD) data, *Remote Sens. Environ.*, 248, 111971, doi:10.1016/j.rse.2020.111971, 2020.

	<b>Fire_cci</b>		Ref.	Fire_cci_D5.1_CAR_v2.1		
	<b>Climate Assessment Report</b>		Issue	2.1	Date	16/11/2020
					Page	45

Nurzahziani, Surussavadee, C. and Noosook, T.: High-Resolution Biomass Burning Aerosol Transport Simulations in the Tropics, *Atmosphere*, 11(1), 91, doi:10.3390/atmos11010091, 2020.

Osborne, C. P., Charles-Dominique, T., Stevens, N., Bond, W. J., Midgley, G. and Lehmann, C. E. R.: Human impacts in African savannas are mediated by plant functional traits, *New Phytol.*, 220(1), 10–24, doi:10.1111/nph.15236, 2018.

Pan, X., Ichoku, C., Chin, M., Bian, H., Darmenov, A., Colarco, P., Ellison, L., Kucsera, T., da Silva, A., Wang, J., Oda, T. and Cui, G.: Six global biomass burning emission datasets: intercomparison and application in one global aerosol model, *Atmospheric Chem. Phys.*, 20(2), 969–994, doi:10.5194/acp-20-969-2020, 2020.

Pino-Cortés, E., Carrasco, S., Díaz-Robles, L. A., Cubillos, F., Vallejo, F., Cereceda-Balic, F. and Fu, J.: Emission Inventory Processing of Biomass Burning from A Global Dataset for Air Quality Modeling, preprint, *EARTH SCIENCES.*, 2020.

Randerson, J. T., Chen, Y., Werf, G. R. van der, Rogers, B. M. and Morton, D. C.: Global burned area and biomass burning emissions from small fires, *J. Geophys. Res. Biogeosciences*, 117(G4), doi:10.1029/2012JG002128, 2012.

Ratnam, J., Bond, W. J., Fensham, R. J., Hoffmann, W. A., Archibald, S., Lehmann, C. E. R., Anderson, M. T., Higgins, S. I. and Sankaran, M.: When is a ‘forest’ a savanna, and why does it matter?, *Glob. Ecol. Biogeogr.*, 20(5), 653–660, doi:10.1111/j.1466-8238.2010.00634.x, 2011.

Roteta, E., Bastarrika, A., Padilla, M., Storm, T. and Chuvieco, E.: Development of a Sentinel-2 burned area algorithm: Generation of a small fire database for sub-Saharan Africa, *Remote Sens. Environ.*, 222, 1–17, doi:10.1016/j.rse.2018.12.011, 2019.

Saide, P. E., Peterson, D. A., da Silva, A., Anderson, B., Ziemba, L. D., Diskin, G., Sachse, G., Hair, J., Butler, C., Fenn, M., Jimenez, J. L., Campuzano-Jost, P., Perring, A. E., Schwarz, J. P., Markovic, M. Z., Russell, P., Redemann, J., Shinozuka, Y., Streets, D. G., Yan, F., Dibb, J., Yokelson, R., Toon, O. B., Hyer, E. and Carmichael, G. R.: Revealing important nocturnal and day-to-day variations in fire smoke emissions through a multiplatform inversion: MULTIPLATFORM INVERSION OF FIRE EMISSION, *Geophys. Res. Lett.*, 42(9), 3609–3618, doi:10.1002/2015GL063737, 2015.

Scholes, R. J., Archibald, S. and von Malitz, G.: Emissions From Fire in Sub-Saharan Africa: The Magnitude of Sources, their Variability and Uncertainty, *Glob. Environ. Res.*, 15, 53–63, 2011.

Schuch, D. A., Ibarra, S., Dias de Freitas, E. and de Fatima Andrade, M.: EmissV: A preprocessor for WRF-Chem model, *J. Atmospheric Sci. Res.*, 1(1), doi:10.30564/jasr.v1i1.347, 2019.

Seiler, W. and Crutzen, P. J.: Estimates of gross and net fluxes of carbon between the biosphere and the atmosphere from biomass burning, *Clim. Change*, 2(3), 207–247, doi:10.1007/BF00137988, 1980.

	<b>Fire_cci</b> <b>Climate Assessment Report</b>		Ref.	Fire_cci_D5.1_CAR_v2.1		
			Issue	2.1	Date	16/11/2020
			Page		46	

Shaffer, L. J.: Indigenous Fire Use to Manage Savanna Landscapes in Southern Mozambique, *Fire Ecol.*, 6(2), 43–59, doi:10.4996/fireecology.0602043, 2010.

Stephens, S. L., Martin, R. E. and Clinton, N. E.: Prehistoric fire area and emissions from California's forests, woodlands, shrublands, and grasslands, *For. Ecol. Manag.*, 251(3), 205–216, doi:10.1016/j.foreco.2007.06.005, 2007.

Tansey, K.: Copernicus Global Land Operations, Vegetation and Energy, CGLOPS-1, Framework Service Contract N° 199494 (JRC), Scientific quality evaluation burned area collection 300m for 2019, version 1. Issue I1.00. [online] Available from: [https://land.copernicus.eu/global/sites/cgls.vito.be/files/products/CGLOPS1\\_SQE2019\\_BA300m-V1\\_I1.00.pdf](https://land.copernicus.eu/global/sites/cgls.vito.be/files/products/CGLOPS1_SQE2019_BA300m-V1_I1.00.pdf) (Accessed 10 January 2020), 2020.

Trentmann, J., Andreae, M. O. and Graf, H.: Chemical processes in a young biomass-burning plume, *J. Geophys. Res. Atmospheres*, 108(D22), 2003JD003732, doi:10.1029/2003JD003732, 2003.

Valencia, A., Venkatram, A., Heist, D., Carruthers, D. and Arunachalam, S.: Development and evaluation of the R-LINE model algorithms to account for chemical transformation in the near-road environment, *Transp. Res. Part Transp. Environ.*, 59, 464–477, doi:10.1016/j.trd.2018.01.028, 2018.

Vara-Vela, A., Andrade, M. F., Kumar, P., Ynoue, R. Y. and Muñoz, A. G.: Impact of vehicular emissions on the formation of fine particles in the Sao Paulo Metropolitan Area: a numerical study with the WRF-Chem model, *Atmospheric Chem. Phys.*, 16(2), 777–797, doi:10.5194/acp-16-777-2016, 2016.

Wang, J., Yue, Y., Wang, Y., Ichoku, C., Ellison, L. and Zeng, J.: Mitigating Satellite-Based Fire Sampling Limitations in Deriving Biomass Burning Emission Rates: Application to WRF-Chem Model Over the Northern sub-Saharan African Region: Reduce fire emission sampling error, *J. Geophys. Res. Atmospheres*, 123(1), 507–528, doi:10.1002/2017JD026840, 2018.

Wang, L., Bartlett, P., Pouliot, D., Chan, E., Lamarche, C., Wulder, M. A., Defourny, P. and Brady, M.: Comparison and Assessment of Regional and Global Land Cover Datasets for Use in CLASS over Canada, *Remote Sens.*, 11(19), 2286, doi:10.3390/rs11192286, 2019.

Wees, D. van and van der Werf, G. R.: Modelling biomass burning emissions and the effect of spatial resolution: a case study for Africa based on the Global Fire Emissions Database (GFED), *Geosci. Model Dev.*, 12(11), 4681–4703, doi:https://doi.org/10.5194/gmd-12-4681-2019, 2019.

van der Werf, G. R., Randerson, J. T., Giglio, L., Collatz, G. J., Kasibhatla, P. S. and Arellano, A. F.: Interannual variability in global biomass burning emissions from 1997 to 2004, *Atmospheric Chem. Phys.*, 6(11), 3423–3441, doi:10.5194/acp-6-3423-2006, 2006.

van der Werf, G. R., Randerson, J. T., Giglio, L., Collatz, G. J., Mu, M., Kasibhatla, P. S., Morton, D. C., DeFries, R. S., Jin, Y. and van Leeuwen, T. T.: Global fire emissions and the contribution of deforestation, savanna, forest, agricultural, and peat fires (1997–

	<b>Fire_cci</b> <b>Climate Assessment Report</b>		Ref.	Fire_cci_D5.1_CAR_v2.1		
			Issue	2.1	Date	16/11/2020
					Page	47

2009), *Atmospheric Chem. Phys.*, 10(23), 11707–11735, doi:10.5194/acp-10-11707-2010, 2010.

van der Werf, G. R., Randerson, J. T., Giglio, L., van Leeuwen, T. T., Chen, Y., Rogers, B. M., Mu, M., van Marle, M. J. E., Morton, D. C., Collatz, G. J., Yokelson, R. J. and Kasibhatla, P. S.: Global fire emissions estimates during 1997–2016, *Earth Syst. Sci. Data*, 9(2), 697–720, doi:10.5194/essd-9-697-2017, 2017.

Wiedinmyer, C., Akagi, S. K., Yokelson, R. J., Emmons, L. K., Al-Saadi, J. A., Orlando, J. J. and Soja, A. J.: The Fire INventory from NCAR (FINN): a high resolution global model to estimate the emissions from open burning, *Geosci. Model Dev.*, 4(3), 625–641, doi:10.5194/gmd-4-625-2011, 2011.

Williams, J. E., Weele, M. van, Velthoven, P. F. J. van, Scheele, M. P., Lioussé, C. and Werf, G. R. van der: The Impact of Uncertainties in African Biomass Burning Emission Estimates on Modeling Global Air Quality, Long Range Transport and Tropospheric Chemical Lifetimes, *Atmosphere*, 3(1), 132–163, doi:10.3390/atmos3010132, 2012.

World Health Organization, R. O. for E.: *Air quality guidelines for Europe*, 2nd ed., Copenhagen : WHO Regional Office for Europe., 2000.

Yokelson, R. J., Griffith, D. W. T. and Ward, D. E.: Open-path Fourier transform infrared studies of large-scale laboratory biomass fires, *J. Geophys. Res. Atmospheres*, 101(D15), 21067–21080, doi:10.1029/96JD01800, 1996.

Yokelson, R. J., Christian, T. J., Karl, T. G. and Guenther, A.: The tropical forest and fire emissions experiment: laboratory fire measurements and synthesis of campaign data, *Atmospheric Chem. Phys.*, 8(13), 3509–3527, doi:10.5194/acp-8-3509-2008, 2008.

Zhang, F., Wang, J., Ichoku, C., Hyer, E. J., Yang, Z., Ge, C., Su, S., Zhang, X., Kondragunta, S., Kaiser, J. W., Wiedinmyer, C. and da Silva, A.: Sensitivity of mesoscale modeling of smoke direct radiative effect to the emission inventory: a case study in northern sub-Saharan African region, *Environ. Res. Lett.*, 9(7), 075002, doi:10.1088/1748-9326/9/7/075002, 2014.

Zubkova, M., Boschetti, L., Abatzoglou, J. T. and Giglio, L.: Changes in Fire Activity in Africa from 2002 to 2016 and Their Potential Drivers, *Geophys. Res. Lett.*, 46(13), 7643–7653, doi:10.1029/2019GL083469, 2019.

## Annex 1: Acronyms and abbreviations

AGL	Agricultural livestock sector
AGRI	Agriculture (residues)
AGS	Agricultural soil sector
ASCII	American Standard Code for Information Interchange
AWS	Agricultural waste burning sector
AMMABB	African Monsoon Multidisciplinary Analysis Biomass Burning
AOD	Aerosol Optical Depth
BA	Burned Area
BC	Black Carbon
BORF	Boreal Forest
CAMS	Copernicus Atmosphere Monitoring Service
CAMS41	CAMS-ANTHRO v4.1 inventory
CAR	Climate Assessment Report
CASA	Carnegie-Ames-Stanford-Approach
CCI	Climate Change Initiative
CGLS	Copernicus Global Land Service
CO	Carbon monoxide
DACCIWA	Dynamics-Aerosol-Chemistry-Cloud Interactions in West Africa
DEFO	Deforestation
ECV	Essential Climate Variables
EDGAR432	Emissions Database for Global Atmospheric Research v4.3.2 inventory
EF	Emission Factor
ESA	European Space Agency
FC	Fuel Consumption
FEER	Fire Energetics and Emissions Research
FINN	Fire INventory from NCAR
FireCCI51	MODIS Fire_cci v5.1
FireCCISFD11	Sentinel-2 SFD Fire_cci v1.1
FREM	Fire Radiative Energy Emissions
FRP	Fire Radiative Power
FRY	FiRe patch morphologY
GFA	Global Fire Atlas
GFAS	Global Fire Assimilation System
GFED	Global Fire Emissions Database
GFED4s	Global Fire Emissions Database version 4, including small fires
GOES	Geostationary Operational Environmental Satellites
GSAV	Grassland SAVanna
HS	Hotspots
JAS	July to September

L3JRC	Global Multi-year (2000-2007) Validated Burnt Area Product
MCD64A1	MODIS Collection 6 Burned Area Product
MODIS	Moderate Resolution Imaging Spectroradiometer
MOPITT	Measurement of Pollution in the Troposphere
MSI	MultiSpectral Instrument
NCAR	National Center for Atmospheric Research
NHAF	Northern Hemisphere Africa
NoP	Number of patches
NOx	Nitrogen oxides
OC	Organic Carbon
PM	Particulate Matter
PM10	PM smaller than 10 µm aerodynamic diameter
PM2.5	PM smaller than 2.5 µm aerodynamic diameter
PROBA-V	Proba Vegetation
QFED	Quick Fire Emissions Dataset
S2	Sentinel-2
S-NPP	Suomi – National Polar-orbiting Partnership
SAVA	Savanna
SFD	Small Fire Dataset
SHAF	Southern Hemisphere Africa
TEMF	Temperate Forest
TRO	Road transport sector
TROF	Tropical forest
VIIRS	Visible Infrared Imaging Radiometer Suite
WF_ABBA	Wildfire Automated biomass Burning Algorithm
WRF-Chem	Weather Research and Forecasting model coupled with Chemistry
WSAV	Woody SAVanna